Ab initio computational analysis of spectral properties of dielectric spheroidal resonators interacting with a subwavelength nanoparticle

Vladimir Shuvayev and Lev Deych

Phys. Rev. E **99**, 013310 — Published 22 January 2019

DOI: 10.1103/PhysRevE.99.013310

An ab initio computational analysis of spectral properties of dielectric spheroidal resonators interacting with a subwavelength nanoparticle.

Vladimir Shuvayev[1] and Lev Deych[1,2]

[1]Physics Department, Queens College of CUNY, Flushing NY 11367

[2]The Graduate Center of CUNY, New York NY 10016

An efficient numerical method for determining the spectral characteristics and spatial distribution of the field of a spheroidal whispering-gallery-mode (WGM) resonator interacting with a dielectric nanoparticle is presented. The developed approach is based on a combination of T-matrix formalism applied to a single resonator with a dipole approximation for the field of the nanoparticle. The method is illustrated by computation of the scattered field of the resonator-particle system illuminated by an incident field in the form of a single WGM mode of TE or TM polarization mimicking the excitation of the resonances by a tapered fiber. Our calculations show that even a very small (less than 0.1%) deviation of the resonator's shape from an ideal sphere renders spherical approximation invalid. They also confirm that analytical resonant approximation for spheroidal resonators developed previously gives a reasonable qualitative description of the spectral characteristics of the resonator-particle system. It was found, however, that corrections to the resonant approximation are significant enough for realistic nominally spherical resonators to be taken into account for accurate analysis of the experimental data.

PACS number(s): 42.25.Bs, 42.25.Fx, 42.60.Da

I. INTRODUCTION

The problem of interaction between Whispering-Gallery-Modes (WGM) of dielectric optical resonators [1,2] and a small subwavelength object placed in the vicinity of the resonator's surface has recently attracted a great deal of attention in a number of areas of fundamental and applied research. More specifically, shifts and broadening of the frequencies of WGMs due to such an interaction have been used to develop novel optical sensors of chemical and biological nanoobjects [3–20] as well as to track the movement of individual atoms in cavity QED experiments [21]. The nanoparticle-induced modification of the spatial profile of the field of WGMs [22,23] has attracted an interest for such applications as WGM based light sources [22,24,25], optical antennas [26], optical manipulation [27–29] and sensing [23].

These works need to be distinguished from another growing area, in which the main attention is being paid to optical resonances of high refractive index dielectric particles of nanometer size [30–35]. While these particles do exhibit distinct resonances in their electro-dipole and magneto-dipole responses, which present a great deal of interest, these resonances are distinct from the Whispering Gallery Modes studied in this paper. The latter can only be realized in relatively large (tens or hundreds of micrometers in size) dielectric objects and correspond to Mie resonances of relatively high order (typical values of the orbital momentum of these resonances can be anywhere between 20 and 400). In principle, it can be of interest in studying the optical interaction between high order Whispering Gallery Mode resonances and magneto-

dipole resonances of nanoparticles with high refractive index, but this study is outside of the scope of this paper[1].

Depending upon relation between the strength of the particle-WGM interaction and the spectral width of the corresponding resonance, the particle-related modification of the resonance frequencies of the system can be described either as splitting of the resonances [16,36–38], when a particle splits a single WGM resonance into two spectrally well-separated resonances, or as a frequency shift, when the experiment reveals that the particle merely shifts a WGM from its original position [12,14,15,39–41]. Theoretically, these effects have been successfully described by two different heuristic models. The splitting is explained by an interaction between two degenerate counter-propagating modes of the resonator with a polarizable dipole [38,42–45], while the shift is modeled by a simple first-order perturbation theory-like expression called Reactive Sensing Principle [39], which was derived under the assumption that in the case of strongly overlapping resonances their degenerate nature is not important.

Despite the success of these models, one would still want to compliment them with more rigorous theories based on Maxwell equations. Such treatments have been developed for two-dimensional disk [22,46,47] and three-dimensional spherical resonator [48–50]. They revealed the polarization dependence of the particle-induced spectral effects, provided relations between phenomenological parameters of the heuristic models and material characteristics of the resonators, as well as allowed to predict the spatial distribution of the electromagnetic field of the resonator-particle system.

The problem is, however, that even nominally spherical resonators with deviations from spherical shape less that 3% are not spherical enough from the point of view of interaction between WGMs and the nanoparticle. Two characteristic energy scales determining a "sphericity" of the resonator are the spectral distance between resonances split due to the shape deformation on one hand, and the particle-induced modifications of the frequencies, on the other. In a typical experiment with "spherical" resonators interacting with a nanoparticle, the former scale significantly exceeds the latter making the assumption of the spherical shape for the resonators inapplicable. It should not come as a surprise, therefore, that the theoretical predictions for the frequencies of the particle-induced resonances obtained in Refs. [48,49] deviate from the experimental data by orders of magnitude[2].

To obtain a description of the WGM-nanoparticle interaction in realistic nominally "spherical" resonators one has to take into account their actual shape. The simplest example of a such "almost" spherical resonator would be a dielectric spheroid. In addition to providing a microscopic theoretical foundation for the phenomenological models of Refs. [38] and [40], and uncovering possible new experimentally relevant effects, a solution to this problem also presents

[1] The study of this problem is currently under way and its results will be reported in a separate publication.

[2] The "reconciliation" of this approximation with experiments attempted in Ref. [50] is based on unrealistic assumptions about exciting field and is, therefore, superficial.

a significant interest for theoretical and computational electrodynamics. Indeed, a rigorous *ab initio* theoretical description and simulation of the spectral effects due to the WGM-nanoparticle interaction in spheroidal resonators is rather challenging. First of all, one should note that the WGMs with high enough Q-factors are characterized by significantly small, compared to the characteristic size of the resonator, wavelength. Accordingly, discretization procedures, which are central to standard simulation tools such as Finite Element (FEM) [51] and Finite Difference Time Domain (FDTD) [52] methods, have to introduce a very fine grid covering relatively large regions of space. This circumstance, by itself, results in significantly increased demands on the amount of memory required for computation and on computational time, making solution of full three-dimensional problems unrealistic [53]. While the axial symmetry of an individual spheroid resonator allows reducing dimensionality of the problem, which makes the situation manageable, in the presence of a nanoparticle the axial symmetry of the problem is destroyed. As a result, one is left with a fully three-dimensional vectorial electrodynamics problem for objects larger than the characteristic wavelengths, which is not susceptible to traditional numerical methods. It is not surprising, therefore, that there have been, to the best of our knowledge, only a single attempt to model numerically the effects of a nanoparticle on WGMs. The authors of Ref. [54] used FEM to simulate the interaction of a nanoparticle with a toroidal resonator, but, in order to make the problem tractable, they had to introduce a simplifying assumption that the particle affects the field of the resonator only in its immediate vicinity. While this computation provided some information on the perturbation of the field of the WGM by the nanoparticle, this approach is not sufficient to study modifications of the spectral properties of the resonator.

The objective of this paper is to present a computationally efficient and accurate *ab initio* approach to computing resonance frequencies and corresponding electric and magnetic fields for spheroidal resonators interacting with a nanoparticle, described as a polarizable dipole. We overcome the inherent difficulties in simulating such systems by combining rigorous Extended Boundary Condition method (EBCM), used to study scattering of light from a single resonator [53,55–61] with a dipole approximation (the only approximation used in this approach) for the field scattered by the particle. The solution of the single resonator scattering problem is presented in the form of the so-called T-matrix [62], which connects expansion coefficients of the scattered field expanded in terms of the vector spherical harmonics (VSH) with corresponding coefficients of the incident field. While the method of the T-matrix had been widely used for scattering studies [58–61,63,64], its application to the WGMs has been so far rather limited. At the same time, the WGMs obviously emerge in various characteristics of the scattered field as resonances (sometimes, especially in the case of spherical scatterers, called Mie resonances), whose position and width contain all the necessary information about the WGMs. Moreover, in many experimental situations, it is the scattering resonances that are being observed and studied. The main concern with applications of the T-matrix formalism to studying WGMs is a poor convergence of this approach in the case of objects much larger than the respective wavelength and/or deviating strongly from the spherical shape [60]. Nevertheless, in the case of scatterers whose shapes do not differ too much from spherical (such as spheroids with

an aspect ratio close to unity), WGM resonances of relatively high order can be found and studied using the T-matrix approach.

We show that using elements of T-matrix as pre-computed parameters and limiting the multipole expansion for the field scattered by the particle to only dipole terms we are able to effectively compute the field scattered by the entire resonator-particle system. The spectral characteristics of this system are studied by identifying resonances of the scattered power in contrast with other approaches describing the problem in terms of the eigenfrequencies and normal modes of the resonator [38,65,66].

This work is an extension of our earlier efforts, where we used a similar idea to obtain a semi-analytical description of the resonator-particle system in the so-called resonance approximation, which takes into account the interaction of the particle with only two remaining degenerate modes of a spheroidal resonator [67,68]. Now we are going outside of the resonant approximation and include into the consideration all modes of the system until convergence of the corresponding sums is achieved. This extension allows us to consider resonators with both very small and relatively large deviations from the spherical shape. One of the most interesting results presented in this paper is the prediction of a drastic (orders of magnitude) and sharp decrease of the particle-induced spectral effects when the deviation from sphericity exceeds some critical value. Our calculations also revealed possible deviations from the resonant approximation due to spectral proximity of the non-resonant modes. Finally, approach developed in this work provides researchers with a robust and efficient computational tool for studying spectral and spatial properties of the resonator-dipole systems. The approach developed here can be extended to include magneto-dipole contribution to the particle field, which might become important for nanoparticles with high enough refractive index [30,69–71].

The structure of this paper is as follows. For convenience of the readers, we begin by describing the T-matrix formalism for a single resonator and present the main properties of the T-matrix in Section II.A. In Section II.B we introduce the dipole approximation for the nanoparticle and derive the main system of equations for the expansion coefficients of the scattered field. Section III is devoted to the description of the numerical procedure used to solve the system of equations derived in Section II.B and to the results of the numerical calculations.

II. INTERACTION BETWEEN WGMS OF A SPHEROIDAL RESONATOR AND A SUBWAVELENGTH PARTICLE: GENERAL THEORY

A. T-matrix formalism for a single spheroidal resonator

We consider a spheroidal resonator interacting with a subwavelength particle positioned in its vicinity. The deviation of the resonator's shape from spherical is characterized by the ellipticity parameter $e = 1 - R_{\mathrm{sm}} / R_r$ (see Figure 1). The field scattered by the resonator is found using the T-matrix formalism, which has been successfully applied in the past to the problem of the

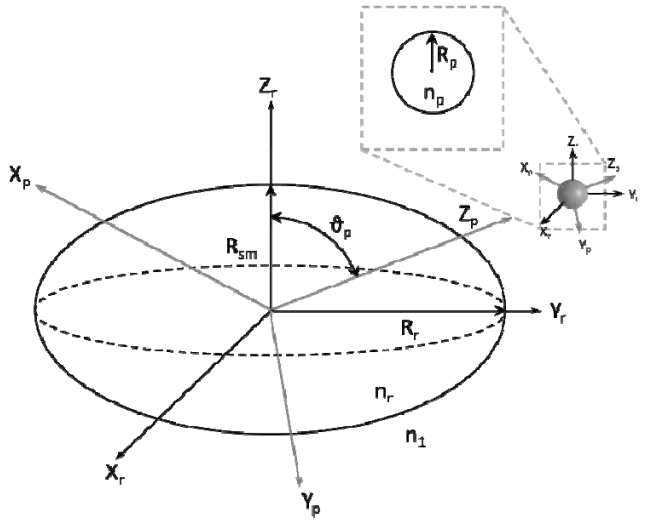

FIG. 1. The resonator-particle system with all its geometric and material parameters: refractive indexes of the resonator, n_r, particle, n_p, and the surrounding medium, n_1; resonator's equatorial radius R_r, its smallest half-axis R_{sm}, and particle's radius R_p. Also shown are four coordinate systems used in the paper: resonator-centered and particle-centered resonator's and particle's systems. Resonator's systems are characterized by the polar (*Z*) axis directed parallel to the axis of rotation of the resonator, while particle's systems have their polar axes directed along a line connecting centers of the particle and the resonator.

scattering of light from non-spherical particles [58–61,63,64]. This formalism is based on presenting the field scattered by the resonator as a linear combination of Vector Spherical Harmonics (VSH) with asymptotic behavior of outgoing spherical waves [62]

$$\mathbf{E}_{sc}^{(r)} = \sum_{l>1} \sum_{|m|\le l} \left[c_{m,l} \mathbf{M}_{m,l}^{(3)}(k_1 r_r, \theta_r, \varphi_r) + g_{m,l} \mathbf{N}_{m,l}^{(3)}(k_1 r_r, \theta_r, \varphi_r) \right], \tag{1}$$

where $\mathbf{M}_{m,l}^{(3)}(k_1 r_r, \theta_r, \varphi_r)$ and $\mathbf{N}_{m,l}^{(3)}(k_1 r_r, \theta_r, \varphi_r)$ are vector spherical harmonics of TE and TM polarizations, respectively, with radial dependence characterized by outgoing spherical Hankel functions $h_l^{(1)}(k_1 r_r)$ of the first kind. Electric field described by a TE polarized VSH and magnetic field described by TM polarized VSH have zero radial components. Modal indexes m and l determine the angular behavior of VSH defined in a spherical coordinate system with a particular choice of its polar (*Z*) axis. We will refer to index l as to orbital number, and, following Ref. [12], will call m, which takes on values in the interval $-l \le m \le l$, the polar index. Arguments r_r, θ_r, φ_r are the radial, polar and azimuthal coordinates of the position vector $\mathbf{r}$ in a particular coordinate system, where subscript r indicates that the origin of the coordinate system is at the center of the resonator. Parameter k_1 is the wavenumber of light outside of the resonator and is defined as $k_1 = n_1 k$, where $k = \omega / c$ is the wave number of electromagnetic field with frequency ω in vacuum, n_1 is the refractive index of the medium surrounding the resonator, and c, as usual, represents the speed of light in vacuum.

Strictly speaking, representation of the scattered field in the form of Eq. (1) is valid only outside of the sphere completely circumscribing the resonator but keeping the particle outside. Assumption that the same expansion is also valid in the immediate vicinity of the scattering object is known as Rayleigh hypothesis [72,73]. While this hypothesis has been studied for a number of scatterers and surfaces [59,74–79], its general validity has not yet been established. However, in the case of a weakly spheroidal resonator, which is a convex body, there are no physical reasons to expect that the scattered field would contain an admixture of VSH with radial dependence of incoming spherical waves. Therefore, we will extend the representation of the scattered field in the form of Eq. (1) throughout the entire exterior of the resonator.

Expansion coefficients $c_{m,l}$ and $g_{m,l}$ in Eq. (1) can be related to the expansion coefficients of the incident field presented as

$$\mathbf{E}_{inc}^{(r)} = \sum_{l>1} \sum_{|m|\le l} \left[a_{m,l} \mathbf{M}_{m,l}^{(1)}(k_1 r_r, \theta_r, \varphi_r) + b_{m,l} \mathbf{N}_{m,l}^{(1)}(k_1 r_r, \theta_r, \varphi_r) \right], \tag{2}$$

where superscript (1) signifies that the radial dependence of the respective VSHs is given by spherical Bessel functions that are regular at the origin. Obviously, the relation between coefficients $c_{m,l}, g_{m,l}$ and $a_{m,l}, b_{m,l}$ is linear and can be presented in the form

$$\begin{aligned} c_{m,l} &= \sum_{\nu\ge 1} \sum_{|\mu|\le \nu} \left[T_{m,l;\mu,\nu}^{(1,1)} a_{\mu,\nu} + T_{m,l;\mu,\nu}^{(1,2)} b_{\mu,\nu} \right] \\ g_{m,l} &= \sum_{\nu\ge 1} \sum_{|\mu|\le \nu} \left[T_{m,l;\mu,\nu}^{(2,1)} a_{\mu,\nu} + T_{m,l;\mu,\nu}^{(2,2)} b_{\mu,\nu} \right] \end{aligned}, \tag{3}$$

where coefficients $T_{m,l;\mu,\nu}^{(\sigma,\sigma')}$ form what is called the T-matrix. Superscripts σ, σ' refer to contribution of VSH of different (TM and TE) polarizations with $\sigma = 1$ corresponding to TE, and $\sigma = 2$ - to TM polarization. Subscripts correspond to two different sets of orbital (l, ν) and polar (m, μ) indexes characterizing individual VSHs.

For a spherical resonator, the T-matrix becomes diagonal in all its indexes and loses its dependence on the polar numbers m, μ:

$$T_{m,l;\mu,\nu}^{(\sigma,\sigma')} = \alpha_l^{(\sigma)}(x) \delta_{l,\nu} \delta_{m,\mu} \delta_{\sigma,\sigma'}. \tag{4}$$

Here $\alpha_l^{(\sigma)}(x)$ are the standard Lorenz-Mie coefficients expressed as functions of the dimensionless size parameter $x = kR_r$, which has the meaning of the number of the vacuum wavelengths per circumference of the sphere with radius R_r. The Lorentz-Mie coefficients can be written down as

$$\alpha_l^{(\sigma)}(x) = -\frac{\varsigma_l^{(\sigma)}(x)}{\varsigma_l^{(\sigma)}(x) + i\beta_l^{(\sigma)}(x)}, \tag{5}$$

where functions $\beta_l^{(\sigma)}(x)$ and $\varsigma_l^{(\sigma)}(x)$ are defined in the Appendix A. The frequencies of WGM resonances in spherical resonators are found from equations $\beta_l^{(\sigma)}(x) = 0$ for both TE and TM polarizations. Solutions of these equations, $x_{l,s}^{(\sigma)}$, are characterized by two (in addition to the polarization) indexes: polar index l, and radial index s distinguishing between resonances with different radial dependences of their respective modes. Resonances are also characterized by their widths, $\gamma_{l,s}^{(\sigma)}$, determined by the behavior of functions $\beta_l^{(\sigma)}, \varsigma_l^{(\sigma)}$ in the vicinity of the respective resonance frequency $x_{l,s}^{(\sigma)}$. Frequency $x_{l,s}^{(\sigma)}$ and width $\gamma_{l,s}^{(\sigma)}$ define the position of the complex pole $x_{l,s}^{(\sigma)} - i\gamma_{l,s}^{(\sigma)}$ in the lower half-plane of the complex plane of x, which can be found by direct solution of equation $\varsigma_l^{(\sigma)}(x) + i\beta_l^{(\sigma)}(x) = 0$. It should be noted that due to complete spherical symmetry Mie coefficients defined by Eq. (5) do not depend on the modal number m and, as a result, all resonances of spherical resonators are $2l+1$ degenerate. At the resonance $x = x_{l,s}^{(\sigma)}$, the Lorenz-Mie coefficients take value $\alpha_l^{(\sigma)}\left[x_{l,s}^{(\sigma)}\right] = -1$, which means that WGM resonances are of pure Breit-Wigner type and that in a vicinity of the resonance frequency the Lorenz-Mie coefficients can be approximated as

$$\alpha_l^{(\sigma)} \approx -\frac{i\gamma_{l,s}^{(\sigma)}}{x - x_{l,s}^{(\sigma)} + i\gamma_{l,s}^{(\sigma)}}. \tag{6}$$

When the shape of a resonator is distorted from spherical to spheroidal, the complete spherical symmetry is replaced with axial symmetry with respect to rotations around the axis of rotation of the spheroid. As a result, the T-matrix acquires non-diagonal elements with respect to all its indices. However, if the VSHs in Eq. (1) and (2) are written in terms of spherical coordinates defined in a coordinate system with polar axes along the axes of rotation (we shall call it the resonator's coordinate system), the T-matrix remains diagonal with respect to the modal number m:

$$\tilde{T}_{m,l;\mu,\nu}^{(\sigma,\sigma')} = \tilde{T}_{m,l;m,\nu}^{(\sigma,\sigma')}\delta_{m,\mu}. \tag{7}$$

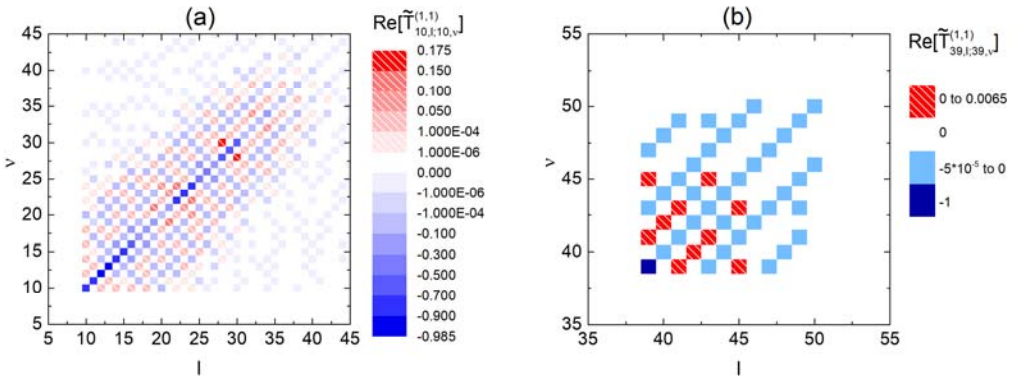

FIG. 3. Real part of various diagonal and non-diagonal elements of the T-matrix $\tilde{T}^{(1,1)}_{10,l;10,\nu}$ (a) and $\tilde{T}^{(1,1)}_{39,l;39,\nu}$ (b) computed for the same frequency corresponding to a second radial order resonance of $\tilde{T}^{(1,1)}_{39,l;39,\nu}$ and $e = 0.048$.

(In what follows, we will use $\tilde{T}$ to designate T-matrix written in the resonator's coordinate system.) Thus, the deviation from the spherical shape results in two main changes: (i) appearance of the non-diagonal elements, which are responsible for coupling between VSHs of different polarizations (TE and TM) and different numbers l, and (ii) dependence of the diagonal elements of the T-matrix, $\tilde{T}^{(\sigma,\sigma)}_{m,l;m,l}$, on the modal number m. When deviations from the spherical shape are not too large, the latter has the largest impact on the spectral properties of the resonators. Indeed, numerical calculations of the T-matrix show that all non-diagonal elements of T-matrix remain small for ellipticity parameters of the spheroid up to 0.05, which is a typical value for practically available nominally spherical resonators (see Figure 2 where we used color/grayscale coding to indicate values of different elements of the T-matrix. The horizontal and vertical axes in this plot represent orbital numbers l and ν in the T-matrix given in Eq. (7), so that the squares along the main diagonal in this figure correspond to $l = \nu$ elements of the T-matrix, while the squares off

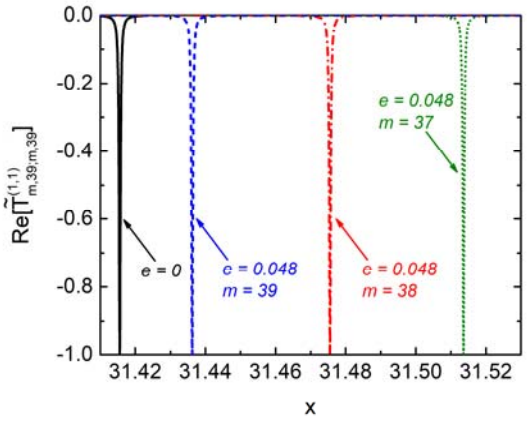

FIG. 2. Real part of a diagonal element of the T-matrix $\tilde{T}^{(1,1)}_{m,39;m,39}$ as a function of the size parameter x. Black solid line corresponds to the spherical resonator with $2l+1$ degenerate polar modes ($e = 0$). Colored dashed and dotted lines depict several resonances of a spheroidal resonator ($e = 0.048$) with same orbital number $l = 39$ and different polar numbers m. Note that at the resonance the real part of the diagonal element of the T-matrix is very close to -1 in both spherical and spheroidal cases.

the main diagonal represent the non-diagonal elements. One can see from this figure that the off-diagonal elements of the T-matrix remain rather small as compared to the diagonal elements). At the same time, the diagonal elements of the T-matrix still demonstrate resonance behavior characterized by Eq. (6), but with frequency and the width of the resonances now dependent on m (see Figure 3, where we plot the frequency dependence of the real parts of the elements of T-matrix with the same values of $l = v$, but different values of $m = \mu$. One can clearly see the same Lorentz-like resonance shapes of the resonances in the spheroids, but with resonant frequencies dependent on the value of the polar number m).

T-matrix has a number of general properties reflecting various symmetries of the scattering object. They all are well known and can be found, for instance, in Ref. [62]. For the convenience of the readers, they are also summarized in Appendix A to this paper. One of the most important for this work is the transformation property of the T-matrix upon the rotation of a coordinate system. While the T-matrix of the spheroid has its simplest form in the resonator's system, in this work we will also have to use a system of coordinates with the polar axis passing through the centers of the resonator and nanoparticle (we will call it the particle's coordinate system). All coordinate systems used in this work are presented in Figure 1. If the rotation from resonator's to particle's coordinates is described by three Euler's angles α, β and γ (designation of the Euler's angles is the same as in Ref. [62]), the T-matrix in the particle's system, $T^{(\sigma,\sigma')}_{m,l;\mu,\nu}$, is related to the T-matrix in the resonator's system by

$$T^{(\sigma,\sigma')}_{m,l;\mu,\nu} = \sum_{m_1=-\min(l,\nu)}^{m_1=\min(l,\nu)} D^{l}_{m,m_1}(-\gamma,-\beta,-\alpha)\tilde{T}^{(\sigma,\sigma')}_{m_1,l;m_1,\nu} D^{\nu}_{m_1,m}(\alpha,\beta,\gamma)\,, \tag{8}$$

where we took into account that T-matrix in the resonator's system, $\tilde{T}^{(\sigma,\sigma')}_{m_1,l;m_1,\nu}$, is diagonal in the modal indexes m. $D^{\nu}_{m_1,m}(\alpha,\beta,\gamma)$ in Eq. (8) is a Wigner D-matrix, realizing a $2l+1$ -dimensional representation of the rotation operator in the space formed by spherical harmonics with orbital number l. Transition between resonator and particle coordinate systems shown in Figure 1 is described by Euler angles

$$\alpha = \pi/2;\ \beta = -\theta_p;\ \gamma = 0\,, \tag{9}$$

where θ_p is the polar coordinate of the particle in the resonator's coordinate system. In this case, the transformation rule given by Eq. (8) can be expressed as

$$T^{(\sigma,\sigma')}_{m,l;\mu,\nu} = \sum_{m_1=-\min(\nu,l)}^{m_1=\min(\nu,l)} (-1)^{\mu-m_1} d^{(l)}_{m,m_1}(\theta_p)\tilde{T}^{(\sigma,\sigma')}_{m_1,l;m_1,\nu} d^{(\nu)}_{m_1,\mu}(\theta_p)\,, \tag{10}$$

where $d^{(l)}_{m,m_1}\left(\theta_p\right)$ is a d-(small) Wigner matrix. An explicit expression for this quantity is provided in Eq. (B5) of Appendix B, and in derivation of Eq. (10) we used Eq. (B4).

B. The general theory of interaction between the spheroidal resonator and a subwavelength polarizable particle

This is the main section of the paper, in which we derive equations for the expansion coefficients of the field scattered by the resonator, $c_{m,l}$ and $g_{m,l}$. Having found these coefficients, we will be able to determine modified resonance frequencies as well as spatial profile of the field scattered by the resonator-particle system. The main assumption of our theory is that the field scattered by the nanoparticle can be described in the dipole approximation. This approximation is introduced by presenting the field scattered by the nanoparticle as a linear combination of VSHs of TM polarization with orbital number $l=1$ and neglecting contribution from TE polarized VSHs:

$$\mathbf{E}^{(p)}_{sc}=\sum_{|m|\le 1} p_m \mathbf{N}^{(3)}_{m,1}\left(k_1 r_p,\theta_p,\varphi_p\right). \tag{11}$$

It should be noted that VSHs in Eq. (11) are written in the coordinate system centered at the nanoparticle, which is indicated in Eq. (11) by subscript p in r_p,θ_p,φ_p. We will call these coordinates particle-centered and would like to warn readers against confusing it with the particle coordinate system introduced in the previous section. While the former refers to the position of the origin of coordinates, the latter denotes the direction of the polar axis (along the line connecting centers of the resonator and the particle). Similarly, one has to distinguish between the *resonator-centered* coordinates with origin at the resonator's center, and the *resonator coordinates* whose polar axis is parallel to the axis of rotation of the resonator. Both resonator-centered and particle-centered coordinate systems can be either resonator or particle coordinates depending on the orientation of their polar axes (Figure 1).

The field scattered by the particle, $\mathbf{E}^{(p)}_{sc}$, is determined by the total field $\mathbf{E}^{(p)}_{in}\left(\mathbf{r}_p\right)$ incident on it. Taking into account that WGMs are usually excited by a tapered fiber positioned in the immediate vicinity of the resonator, it is reasonable to assume that $\mathbf{E}^{(p)}_{in}\left(\mathbf{r}_p\right)\equiv\mathbf{E}^{(r)}_{sc}\left(\mathbf{r}_r\right)$, where $\mathbf{E}^{(r)}_{sc}$ is the field scattered by the resonator and presented by Eq. (1). This field, however, must be rewritten in the particle-centered rather than in the resonator-centered coordinate system. If these coordinate systems can be transformed to each other by a simple translation, one can convert resonator-centered VSHs into the particle-centered ones and vice versa using vector translational addition theorem [80]. According to this theorem, the resonator-centered VSHs of Eq. (1) can be presented as

$$\mathbf{N}_{m,l}^{(3)}\left(k_1 r_r,\theta_r,\varphi_r\right)=\sum_{\nu=1}^{\infty}\sum_{\mu=-\nu}^{\nu}\Big[A_{\mu,\nu;m,l}^{(+)}\left(k_1,-\mathbf{d}_{pr}\right)\mathbf{N}_{\mu,\nu}^{(1)}\left(k_1 r_p,\theta_p,\varphi_p\right)+ B_{\mu,\nu;m,l}^{(+)}\left(k_1,-\mathbf{d}_{pr}\right)\mathbf{M}_{\mu,\nu}^{(1)}\left(k_1 r_p,\theta_p,\varphi_p\right)\Big],$$
$$\mathbf{M}_{m,l}^{(3)}\left(k_1 r_r,\theta_r,\varphi_r\right)=\sum_{\nu=1}^{\infty}\sum_{\mu=-\nu}^{\nu}\Big[A_{\mu,\nu;m,l}^{(+)}\left(k_1,-\mathbf{d}_{pr}\right)\mathbf{M}_{\mu,\nu}^{(1)}\left(k_1 r_p,\theta_p,\varphi_p\right)+ B_{\mu,\nu;m,l}^{(+)}\left(k_1,-\mathbf{d}_{pr}\right)\mathbf{N}_{\mu,\nu}^{(1)}\left(k_1 r_p,\theta_p,\varphi_p\right)\Big] \quad (12)$$

where $\mathbf{d}_{pr}$ is the position vector of the center of the particle in a resonator-centered coordinate system, $A_{\mu,\nu;m,l}^{(+)}$ and $B_{\mu,\nu;m,l}^{(+)}$ are so-called translation coefficients and superscript (+) indicates that the radial dependence of these coefficients is given by the outgoing spherical Hankel functions. One can see from Eq. (12) that translation coefficients $A_{\mu,\nu;m,l}^{(+)}$ connect VSHs of the same polarization, while coefficients $B_{\mu,\nu;m,l}^{(+)}$ are responsible for the polarization conversion due to translation. In this paper we use the same normalization of the VSH and of the translation coefficients as in Ref. [62] (all relevant expressions are given in Appendix C, Eqs. (C1) through (C4) for VSHs and Eqs. (C5) through (C8) for the translation coefficients). The translation coefficients have useful symmetry properties with respect to inversion of the translation vector $\mathbf{d}_{pr}$ and interchange of the modal indexes [81]:

$$A_{m,l;\mu,\nu}^{(+)}(k_1,-\mathbf{d}_{pr})=\left[A_{\mu,\nu;m,l}^{(-)}(k_1,\mathbf{d}_{pr})\right]^*,\quad B_{m,l;\mu,\nu}^{(+)}(k_1,-\mathbf{d}_{pr})=\left[B_{\mu,\nu;m,l}^{(-)}(k_1,\mathbf{d}_{pr})\right]^* \quad (13)$$

where superscript (-) in translation coefficients on the right-hand side of Eq. (13) indicates that their dependence upon the radial coordinate of the translation vector $\mathbf{d}_{pr}$ is given by incoming spherical Hankel functions $h_l^{(2)}(k_1 d_{pr})$.

Choosing the polar axes of the particle-centered and the resonator-centered coordinates to be parallel to the translation vector $\mathbf{d}_{pr}$ (i.e. assuming that both of them are the particle systems), we make the translation coefficients diagonal with respect to indexes m and μ. This choice of the coordinate axes significantly simplifies calculations and will be used in the rest of this work. Taking into account the explicit form of the translation coefficients, Eq. (C9) in Appendix C, one can show that in the particular case of translation coefficients with $m=\mu$ and one of the polar indexes equal to unity, symmetry relations given by Eq. (13) take the form

$$A_{m,l;m,1}^{(+)}(k_1,-\mathbf{d}_{pr})=A_{m,1;m,l}^{(+)}(k_1,\mathbf{d}_{pr}),\quad B_{m,l;m,1}^{(+)}(k_1,-\mathbf{d}_{pr})=-B_{m,1;m,l}^{(+)}(k_1,\mathbf{d}_{pr}). \quad (14)$$

With help of Eq. (12) we can present Eq. (1) in the form suitable for finding coefficients p_m of Eq. (11). Using the Lorentz-Mie solution for the spherical particles [62] we find:

$$p_m = \alpha_p \sum_{l=1}^{\infty} \left[g_{m,l} A^{(+)}_{m,1;m,l}\left(k_1, -\mathbf{d}_{pr}\right) + c_{m,l} B^{(+)}_{m,1;m,l}\left(k_1, -\mathbf{d}_{pr}\right) \right], \tag{15}$$

where

$$\alpha_p \equiv \alpha_1^{(2)}\left(x\varsigma\right) \tag{16}$$

is an abbreviated notation for the $l=1$ Lorenz-Mie coefficient for TM polarized field of a spherical particle of radius R_p. This coefficient is given by the same expressions as Eq. (5) with resonator's refractive index replaced by particle's index n_p, and resonator's radius by particle's radius R_p. In order to keep the same definition of the size parameter x as in Eq. (5), we introduced into Eq. (16) a parameter $\varsigma = R_p / R_r \ll 1$ characterizing the size of the particle relative to that of the resonator.

Before continuing with the derivation of equations for the field expansion coefficients we must comment on the applicability of the Eq. (11) for the field of the nanoparticle. The approximation expressed by this equation is not equivalent to the uniform field assumption, which is often identified with the dipole approximation. While the latter is valid only if $x\varsigma \ll 1$ and allows replacing the Mie-Lorentz coefficient α_p with the first non-vanishing terms in its expansion with respect to $x\varsigma$:

$$\alpha_p \approx -i\frac{2}{3}\left(n_1 x\varsigma\right)^3 \frac{n_p^2 - n_1^2}{n_p^2 + 2n_1^2}\left[1 + i\frac{2}{3}\left(n_1 x\varsigma\right)^3 \frac{n_p^2 - n_1^2}{n_p^2 + 2n_1^2}\right], \tag{17}$$

the validity of Eq. (11) requires only that Mie-Lorentz coefficient α_p remains much larger than all other coefficients $\alpha_l^{(\sigma)}$ in the spectral region of interest. In the case of WGMs characterized by large values of orbital number, $l \gg 1$, the inequality $x\varsigma \ll 1$ and, hence, validity of Eq. (17), is not at all assured even for very small nanoparticles while Eq. (11) might remain valid even when Eq. (17) is not. To illustrate this point we compare α_p with quadrupole and other higher order coefficients using as an example parameters of the system studied in Ref. [12] ($\varsigma = 0.0058$, $n_1 = 1.326$, $n_r = 1.449$, $n_p = 1.5718$). Taking into account that orbital number of the WGM excited in those experiments was $l = 340$, which corresponds to $x = 242.15$ at the frequency of the WGM resonance, we estimate $x\varsigma \approx 1.39$. Clearly, the uniform field approximation given by Eq. (17) is not valid in this case. At the same time, estimates of the ratio $\alpha_l^{(2)}(x\varsigma)/\alpha_p$ for $l > 1$

produce values $\alpha_2^{(2)}(x\varsigma)/\alpha_p \approx 0.245-0.05i$, $\alpha_3^{(2)}(x\varsigma)/\alpha_p \approx 0.0235-0.006i$ and even smaller values for larger orbital mode numbers. However, one also needs to be aware of the $l=1$ contribution to the particle's field from the TE polarized VSH, which, for such large values of the parameter $x\varsigma$, can become comparable with the dipole TM contribution. For the parameters cited above, we find that $\alpha_1^{(1)}(x\varsigma)/\alpha_p \approx 0.521-0.068i$ and it might have to be taken into account. This contribution can become even more significant in the case of nanoparticles with very high refractive index, which can show a very strong magnetic response [30,69–71]. This is a very interesting possibility, and, in principle, the theory presented in this paper can be generalized to include also the TE contribution to the particle field. However, this is a topic for a separate publication, and here we will stay within the dipole approximation expressed by Eq. (11), whose range of validity is defined by inequality $x\varsigma \le 1$ and is much less restrictive than condition $x\varsigma \ll 1$ required for applicability of the uniform field approximation.

The expansion coefficients of the resonator's scattering field, $g_{m,l}$ and $c_{m,l}$, in the presence of the particle are determined by the same Eq. (3) as in the absence of the particle, where, however, the incident field coefficients $a_{m,l}$ and $b_{m,l}$ should be modified to account for the contribution of the field scattered by the particle into the field incident on the resonator. This is achieved by applying the translational addition theorem to Eq. (11), which allows rewriting this field in the form

$$\mathbf{E}_{sc}^{(p)} = \sum_{|m|\le 1}\sum_{\nu=1}^{\infty}\sum_{\mu=-\nu}^{\nu} p_m \left[A_{\mu,\nu;m,1}^{(+)}\left(k_1,\mathbf{d}_{pr}\right)\mathbf{N}_{\mu,\nu}^{(1)}\left(k_1 r_r,\theta_r,\varphi_r\right) + B_{\mu,\nu;m,1}^{(+)}\left(k_1,\mathbf{d}_{pr}\right)\mathbf{M}_{\mu,\nu}^{(1)}\left(k_1 r_r,\theta_r,\varphi_r\right)\right]. \qquad (18)$$

Combining Eq. (18) with Eq. (2) for the external incident field, we find that in the particle's coordinate system the incident field coefficients $a_{m,l}$ and $b_{m,l}$ in Eq. (3) must be replaced according to:

$$\begin{aligned} a_{m,l} &\Rightarrow a_{m,l} + p_m B_{m,l;m,1}^{(+)}\left(k_1,\mathbf{d}_{pr}\right) \\ b_{m,l} &\Rightarrow b_{m,l} + p_m A_{m,l;m,1}^{(+)}\left(k_1,\mathbf{d}_{pr}\right) \end{aligned}. \qquad (19)$$

At this point, we shall specify the excitation conditions that will be assumed in this work. The most effective excitation of WGMs is achieved by using a tapered fiber positioned in the close proximity of the resonator [82–85]. Strictly speaking, the resonator and the exciting fiber must be considered as a coupled system, in which the field in the fiber not only excites WGMs but also affects their properties, most notably the Q-factor [85–89]. To deal with this situation rigorously one would need to treat coefficients of the incident field as dynamic variables and compliment equations for the field in the resonator with equations describing the field in the fiber. This consideration, however, is outside of the scope of this work, and here we shall treat the expansion coefficients of the incident field as external parameters. We will choose them in a way

that would mimic the excitation in a *spherical* resonator and in the absence of the nanoparticle of a single mode of a given (TE or TM) polarization with a specified orbital number $l = L$ and radial number $s = S$. In the *resonator's coordinate system* such a mode is characterized by a single VSH with modal numbers $m = M;\ l = L$. Thus, the TE illumination conditions are described by the parameters of the incident field chosen as

$$\tilde{a}_{m,l} = a_0 \delta_{m,M} \delta_{l,L}; \tilde{b}_{m,l} = 0, \tag{20}$$

while to describe the TM illumination we postulate

$$\tilde{b}_{m,l} = b_0 \delta_{m,M} \delta_{l,L}; \tilde{a}_{m,l} = 0. \tag{21}$$

Here we again use the tilde to indicate that the respective quantity is written in the resonator's coordinate system. Parameters a_0 and b_0 are normalization coefficients that can be determined from experimental values of power entering the resonator. It should be emphasized that pure TE or pure TM modes cannot be excited in the spheroidal resonators, therefore Eqs. (20) and (21) should not be construed to assume that field actually excited under conditions of Eq. (20) have TE polarization or that the field excited under conditions of Eq. (21) are of TM polarization.

Expansion coefficients of the field transform under rotation from the resonator's to the particle's coordinates characterized by Euler angles α, β, γ as

$$\begin{pmatrix} a_{m,L} \\ b_{m,L} \end{pmatrix} = \sum_{m_1=-L}^{L} D^{(L)}_{m,m_1}(-\gamma, -\beta, -\alpha) \begin{pmatrix} \tilde{a}_{m_1,L} \\ \tilde{b}_{m_1,L} \end{pmatrix}. \tag{22}$$

Taking into account values of the Euler's angles, given by Eq. (9) and Eqs. (20), (21), we can present the expansion coefficients of the incident field in the particle's coordinate system as

$$\begin{pmatrix} a_{m,L} \\ b_{m,L} \end{pmatrix} = (-i)^M d^{(L)}_{m,M}(\theta_p) \begin{pmatrix} a_0 \\ b_0 \end{pmatrix}. \tag{23}$$

Substituting Eq. (19) into Eq. (3) we arrive to the following system of equations for the expansion coefficients of the field scattered by the resonator in the presence of the nanoparticle:

$$\begin{aligned} c^{(\sigma)}_{m,l} &= c^{(\sigma,0)}_{l,m} + \sum_{\nu=1}^{\infty} \sum_{\mu=-1}^{1} \left[T^{(1,1)}_{m,l;\mu,\nu} B^{(+)}_{\mu,\nu;\mu,1}(k_1, \mathbf{d}_{pr}) + T^{(1,2)}_{m,l;\mu,\nu} A^{(+)}_{\mu,\nu;\mu,1}(k_1, \mathbf{d}_{pr}) \right] p^{(\sigma)}_{\mu} \\ g^{(\sigma)}_{m,l} &= g^{(\sigma,0)}_{l,m} + \sum_{\nu=1}^{\infty} \sum_{\mu=-1}^{1} \left[T^{(2,1)}_{m,l;\mu,\nu} B^{(+)}_{\mu,\nu;\mu,1}(k_1, \mathbf{d}_{pr}) + T^{(2,2)}_{m,l;\mu,\nu} A^{(+)}_{\mu,\nu;\mu,1}(k_1, \mathbf{d}_{pr}) \right] p^{(\sigma)}_{\mu} \end{aligned}, \tag{24}$$

where we added superscripts in $c_{m,l}^{(\sigma)}$ and $g_{m,l}^{(\sigma)}$ to distinguish between the two types of the excitation – TE for $\sigma=1$ and TM for $\sigma=2$. Coefficients $c_{l,m}^{(\sigma,0)}$ and $g_{l,m}^{(\sigma,0)}$ are expansion coefficients of the scattered field under TE or TM illuminations in the absence of the nanoparticle:

$$\begin{aligned} c_{l,m}^{(\sigma,0)} &= \sum_{\mu=-L}^{L} T_{m,l;\mu,L}^{(1,\sigma)} a_{\mu,L} = (-i)^M d_{m,M}^{(l)}(\theta_p) \tilde{T}_{M,l;M,L}^{(1,\sigma)} a_0 \\ g_{l,m}^{(\sigma,0)} &= \sum_{\mu=-L}^{L} T_{m,l;\mu,L}^{(2,\sigma)} b_{\mu,L} = (-i)^M d_{m,M}^{(l)}(\theta_p) \tilde{T}_{M,l;M,L}^{(2,\sigma)} b_0 \end{aligned}, \tag{25}$$

where we used transformation properties of the T-matrix, Eq. (10), and of expansion coefficients, Eq. (23).

Using Eq. (24) one can eliminate the resonator's coefficients $c_{m,l}^{(\sigma)}$ and $g_{m,l}^{(\sigma)}$ in Eq. (15) and derive a closed system of equations for particle's coefficients $p_\mu^{(\sigma)}$, where we again added superscript to distinguish between the cases of TE ($\sigma=1$) and TM ($\sigma=2$) illumination conditions:

$$\sum_{\mu=-1}^{1} \left[\delta_{m,\mu} - \alpha_p \left(U_{m,\mu} + V_{m,\mu} \right) \right] p_\mu^{(\sigma)} = \alpha_p \sum_l \left[c_{l,m}^{(\sigma,0)} B_{m,1;m,l}^{(+)} \left(k_1, -\mathbf{d}_{pr} \right) + g_{l,m}^{(\sigma,0)} A_{m,1;m,l}^{(+)} \left(k_1, -\mathbf{d}_{pr} \right) \right]. \tag{26}$$

Matrices $U_{m,\mu}$ and $V_{m,\mu}$ in Eq. (26) are defined as

$$\begin{aligned} U_{m,\mu} &= \sum_\nu \sum_l \left[T_{m,l;\mu,\nu}^{(2,1)} B_{\mu,\nu;\mu,1}^{(+)}(k_1, \mathbf{d}_{pr}) + T_{m,l;\mu,\nu}^{(2,2)} A_{\mu,\nu;\mu,1}^{(+)}(k_1, \mathbf{d}_{pr}) \right] A_{m,1;m,l}^{(+)} \left(k_1, -\mathbf{d}_{pr} \right) \\ V_{m,\mu} &= \sum_\nu \sum_l \left[T_{m,l;\mu,\nu}^{(1,1)} B_{\mu,\nu;\mu,1}^{(+)}(k_1, \mathbf{d}_{pr}) + T_{m,l;\mu,\nu}^{(1,2)} A_{\mu,\nu;\mu,1}^{(+)}(k_1, \mathbf{d}_{pr}) \right] B_{m,1;m,l}^{(+)} \left(k_1, -\mathbf{d}_{pr} \right) \end{aligned}. \tag{27}$$

Since translation coefficients vanish whenever one of the polar numbers m or μ exceeds its respective orbital number l or ν, the only non-zero elements of these matrices correspond to values $|m| \le 1$, $|\mu| \le 1$. This is, of course, fully consistent with the dipole approximation used to describe the field scattered by the particle. In the case of spherical resonators, when the T-matrix becomes diagonal in all its indexes and loses its dependence on the polar number m, matrices $U_{m,\mu}$ and $V_{m,\mu}$ are reduced to the respective expressions of Ref. [48,49]:

$$U_{m,\mu} = \delta_{m,\mu} \sum_l \alpha_l^{(2)} \left[A_{m,l;m,1}^{(+)}(k_1, \mathbf{d}_{pr}) \right]^2; V_{m,\mu} = -\delta_{m,\mu} \sum_l \alpha_l^{(1)} \left[B_{m,l;m,1}^{(+)}(k_1, \mathbf{d}_{pr}) \right]^2, \tag{28}$$

where we used Eq. (4) to represent elements of the T-matrix in terms of the Lorentz-Mie coefficients and took into account properties of the translation coefficients given by Eq. (14).

Derivation of Eq. (26) essentially completes formulation of the general theory of the WGM resonances in spheroidal resonators interacting with a polarizable dipole. Full numerical analysis of the system under consideration involves solution of the system of Eq. (26) and (24), which is quite straightforward, provided that we can compute matrices $U_{m,\mu}$ and $V_{m,\mu}$. They contain products of the off-diagonal components of the T-matrix and the translation coefficients. The T-matrix in the resonator's coordinate system can be computed using one of many publicly available codes, e.g. one presented on the website maintained by M. Mishchenko, Ref. [90], and transformed into the particle's system using transformation rule Eq. (10). The computation of the translation coefficients appearing in Eq. (28) is also quite straightforward with Eq. (C9) and requires only ability to compute Hankel functions. The problem arises for very high values of $L \geq 50$ since in this case the non-diagonal elements of the T-matrix become very small while the translation coefficients become very large. Under these circumstances, it is very easy to lose significant contributions to $U_{m,\mu}$ and $V_{m,\mu}$ if the magnitude of the T-matrix elements drops below the precision limit set for their computation. This difficulty becomes more significant for small particles located very close to the surface of the resonator because in this case in order to reach convergence criteria one has to include terms with higher values of l into respective sums in Eqs. (24) and (26). This problem, however, is not of principle nature and can be overcome by improving computational precision of available T-matrix codes. Using modern computational platforms these calculations can be carried out with arbitrary precision, which will, of course, make the computations longer. In this work, whose main goal is to illustrate the developed approach, we shall limit our consideration to relatively low values of L. At the same time, we showed in Ref. [67] that the WGM with lower orbital orders excited in smaller resonators can result in significantly enhanced particle-related effects. Therefore, consideration of WGMs with smaller orbital numbers present significant interest and the results of this work can be useful beyond mere illustration of the method.

III. INTERACTION BETWEEN WGMS OF A SPHEROIDAL RESONATOR AND A SUBWAVELENGTH PARTICLE: RESULTS

A. Particle-induced modification of the WGM resonance frequencies

In this section we discuss the modification of resonance frequencies of the spheroidal resonator due to interaction with the nanoparticle. This issue has attracted the largest attention in the recent literature (see Introduction for references) due to its importance for WGM-based single particle sensors. In this subsection we will present the results of the numerical computation of these frequencies, which will be compared with the results of approximate analytical calculations based on the resonant approximation [67]. For numerical simulations we choose the resonator-particle system with the following parameters $n_1 = 1$, $n_r = n_p = 1.59$, $R_r = 4\,\mu m$, $R_p = 0.032\,\mu m$, $d_{pr} = 4.2\,\mu m$. The calculations were carried out for excitation conditions of both TE and TM polarizations with exciting field characterized by $L = 39$ and different values of the polar

number M. To compute the frequencies of the modified WGM resonances it is sufficient to consider the expansion coefficients of the particle's scattered field $p_{\mu}^{(\sigma)}$ defined by Eq. (26). The frequencies are found by identifying the resonances of these coefficients.

We begin by computing the dependence of the particle-induced resonance frequencies upon the ellipticity of the resonator e. For this particular computation we assume that the particle is positioned in the equatorial plane of the resonator ($\theta_p = \pi/2$) and study coefficients $p_{\pm 1}^{(\sigma)}$ and $p_0^{(\sigma)}$ as functions of frequency. For TE excitation, we find that coefficients $p_{\pm 1}^{(1)}$ demonstrate resonance behavior with the same resonance frequency for both $p_1^{(1)}$ and $p_{-1}^{(1)}$ coefficients, while the coefficient $p_0^{(1)}$ remains very small for all frequencies. This means that in the case of the TE excitation there exist components of the resonator's field, which do not interact with the particle, and, therefore resonate at the frequency of the initial WGM resonance of the resonator. This conclusion is confirmed by direct calculations of the coefficients $c_{m,l}^{(\sigma)}$ and $g_{m,l}^{(\sigma)}$ of $\mathbf{E}_{sc}^{(r)}(\mathbf{r})$, which will be presented in the next section of the paper. Thus, as expected, the particle induces splitting of a single TE WGM peak in two spectrally close resonances, one of which coincides with the original WGM resonance of a single resonator. This behavior of TE WGMs is related to the properties of the translation coefficient $B_{m,l;m,1}^{(+)}(k_1, \mathbf{d}_{pr})$, which vanishes at $m = 0$ (see Eq. (C9) in Appendix C), and can also be traced to the reflection symmetry of the resonator-particle system with respect of the equatorial plane of the resonator [67].

The results of these calculations for two different values of the resonator-particle distance d_{pr} and TE excitation are shown in Figure 4. One can see that small deviation of the resonator's shape from sphere results in sharp reduction of the splitting $\delta\omega$ expressed in terms of the dimensionless size parameter x. However, after initial decrease, $\delta\omega$ dependence on e saturates so that when the ellipticity exceeds some crossover value e_{cr}, the splitting remains virtually independent of e. The crossover value e_{cr} depends on d_{pr} ($e_{cr} = 0.001$ for $d_{pr} = 4.036\,\mu m$ and $e_{cr} = 2\times 10^{-5}$ for $d_{pr} = 4.2\,\mu m$), but always remains

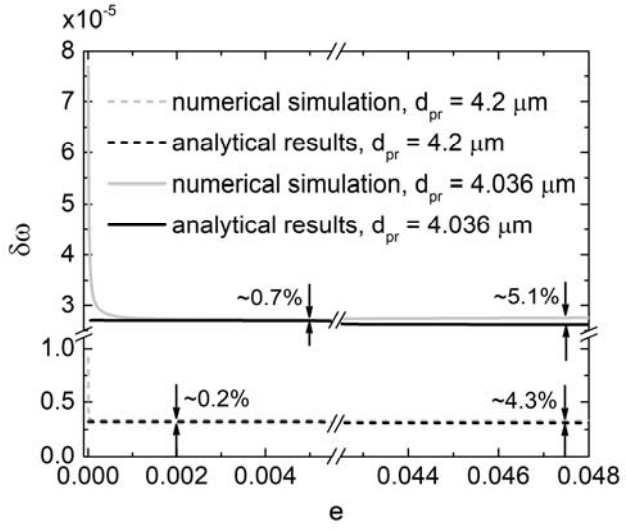

FIG. 4. Dependence of the frequency splitting versus ellipticity of the resonator in case of TE excitation for two resonator-particle distances obtained from coefficients $p_{\pm 1}^{(1)}$. Gray lines (solid and broken) represent results of numerical computation, and black solid and broken lines show results obtained from analytical expressions derived using resonance approximation of Ref. [67].

relatively small that all realistic nominally spherical solid resonators are characterized by ellipticity parameters $e > e_{cr}$. The regime $e < e_{cr}$ can be in principle achieved in liquid droplets actuated as resonators, which recently started attracting significant attention [91–95]. Experiments with liquid droplets controlled by optical tweezers might provide the experimental verification of the effects presented in Figure 4. Physically, the e_{cr} separates two regimes: for $e < e_{cr}$ the particle-induced splitting $\delta\omega$ exceeds the spectral distance $\Delta\omega_{M,L;M\pm1,L}$ between WGMs with the same value of orbital number L and adjacent polar numbers M and $M \pm 1$, while for $e > e_{cr}$ we find that $\delta\omega \approx \Delta\omega_{M,L;M\pm1,L}$. These findings agree with the approximate analytical results presented in Ref. [67] and are also shown in Figure 4. We can also conclude that inequality $1 \gg e > e_{cr}$ can be considered as a condition of applicability of the resonance approximation introduced in Ref. [67].

The resonant response of the resonator-particle system to the TM excitation is different. Now in addition to resonances of $p_{\pm1}^{(2)}$, which occur at coinciding frequencies, we also observe resonance of $p_0^{(2)}$ at a new frequency. The difference between TM and TE excitations can again be explained by the different behavior of TE and TM polarized electric fields with respect to reflection in the equatorial plane. However, the behavior of both these frequencies as functions of ellipticity is similar to that of TE polarization, although the value of e_{cr} is different for each of the two frequencies: it is larger for the resonance of $p_0^{(2)}$ because this resonance is shifted stronger from the original WGM frequency than the one associated with coefficients $p_{\pm1}^{(2)}$ (see Figure 5).

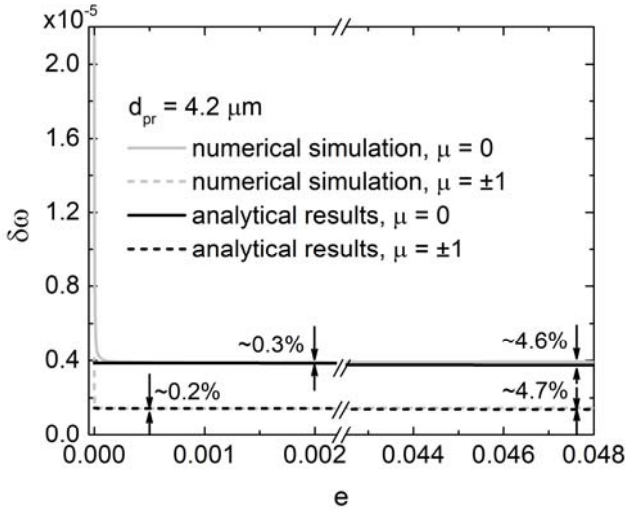

FIG. 5. Dependence of the frequency splitting versus ellipticity of the resonator in case of TM excitation for a single resonator-particle distance obtained from coefficients $p_{\mu}^{(2)}$. Gray lines (solid and broken) represent results of numerical computation, and black solid and broken lines show results obtained from analytical expressions derived using resonance approximation of Ref. [67].

One of the challenges in using observations of the particle-induced shifts WGM resonances for sensing is the lack of control over the position of the analyte particle on the surface of the resonator. It was suggested and demonstrated experimentally in Ref. [12] that one can determine the angular coordinate of the particle by comparing frequency shifts of WGMs with the same orbital, but different polar numbers. It is interesting, therefore, to consider the resonance frequencies as functions of particle's angular coordinate θ_p for various polar modes of the

resonator-particle system comparing the rigorous numerical results with those of the resonant approximation.

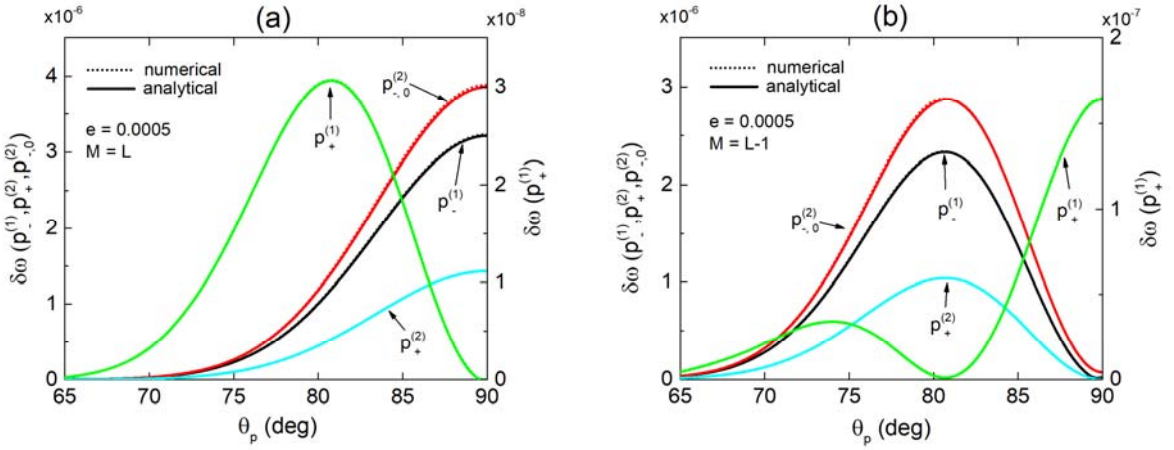

FIG. 6. Angular dependence of the shift of the particle-induced resonance frequencies excited by a TM type ($p_{+}^{(2)}, p_{-,0}^{(2)}$ - left vertical axis) and TE type ($p_{-}^{(1)}$ - left vertical axis and $p_{+}^{(1)}$ - right vertical axis) excitation with $L = 39$ and $M = L$ (a) and $M = L - 1$ (b) obtained by observing maximums of $p_{\pm,0}^{(1,2)}$ coefficients for $e = 0.0005$. The coefficients $p_{+}^{(1)}$ and $p_{-}^{(2)}$ vanish at the equatorial position of the particle on the (a) graph, as well as coefficients $p_{-}^{(1)}$, $p_{0}^{(2)}$ and $p_{+}^{(2)}$ on the (b) graph.

The first thing to note in this regard is that for the off-equatorial position of the particle coefficients $p_{1}^{(1)}, p_{-1}^{(1)}$ for the TE excitation or coefficients $p_{\pm1}^{(2)}, p_{0}^{(2)}$ for the TM excitation do not describe excitation of the normal modes of the resonator-particle system in the sense that they do not resonate at a single frequency. Analytical calculations of Ref. [67] indicate that in this case combinations $p_{\pm}^{(1,2)} = p_{1}^{(1,2)} \pm p_{-1}^{(1,2)}$ represent normal modes for both TE and TM excitation types.

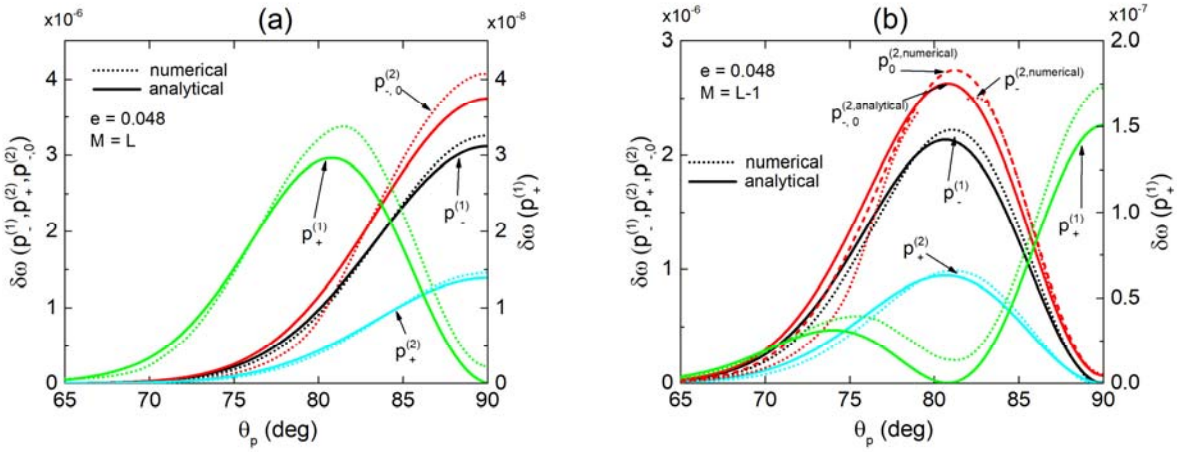

FIG. 7. Angular dependence of the shift of the particle-induced resonance frequencies excited by a TM type ($p_{+}^{(2)}, p_{-,0}^{(2)}$ - left vertical axis) and TE type ($p_{-}^{(1)}$ - left vertical axis and $p_{+}^{(1)}$ - right vertical axis) excitation with $L = 39$ and $M = L$ (a) and $M = L - 1$ (b) obtained by observing maximums of $p_{\pm,0}^{(1,2)}$ coefficients for $e = 0.048$. At the equatorial position of the particle the coefficients $p_{+}^{(1)}$ and $p_{-}^{(2)}$ vanish on the (a) graph, as well as coefficients $p_{-}^{(1)}$, $p_{0}^{(2)}$ and $p_{+}^{(2)}$ on the (b) graph.

In the latter case, the resonant approximation predicts that $p_{-}^{(2)}$ and $p_{0}^{(2)}$ coefficients resonate at the same frequency, the fact confirmed by numerical computations as well. Thus, we computed coefficients $p_{\pm}^{(1,2)}$ and used their frequency dependence to establish positions of the particle-induced resonances for a number of different values of θ_p. In Figure 6 we present the results of these calculations for two values of the exciting polar number $M = L$ and $M = L-1$ for the resonator with a very small ellipticity $e = 0.0005$, which is, however, still larger than the critical value e_{cr} for the equatorial position of the particle (see Figure 3). One can see an excellent agreement between numerical and analytical results based on the resonant approximation of Ref. [67] for both fundamental and $M = L-1$ mode. This means that, even for such a small ellipticity, the particle "sees" only two instead of $2L+1$ degenerate modes in agreement with assumptions of Ref. [67] and results shown in Figure 3, while all off-diagonal and non-resonant elements of the T-matrix indeed remain very small.

However, it is more interesting to compare numerical and analytical results for more realistic values of ellipticity. In Figure 7 we present the results of calculations for $e = 0.048$, which corresponds to typical values for nominally spherical resonators used in sensing experiments. While the magnitude of the shift, compared to the case of smaller ellipticity, does not change much, the difference between numerical and analytical results grows as expected. This difference is growing with deviation of the particle's location from equatorial, but for $M = L-1$ mode and θ_p below ~84 degrees, a new qualitative effect emerges in the frequency dependence of coefficient $p_{-}^{(2)}$. As one can see from Figure 8, coefficient $p_{-}^{(2)}$ acquires an additional maximum at angle $\theta_p = 79^{\circ}$, which grows more prominent for $\theta_p = 77^{\circ}$ and eventually washes out traces of both original maxima resulting in a broad spectral feature not directly related to the resonant frequencies of the system. The origin of this additional maximum can be traced to one of the non-resonant matrix elements of the T-matrix showing the limitations of the resonant approximation and even more so of the heuristic phenomenological models. At the same time this phenomenon does not manifest itself in the behavior of coefficient $p_{0}^{(2)}$, which remains unaffected and can be used instead of $p_{-}^{(2)}$ to locate positions of the resonances (Figure 7(b)).

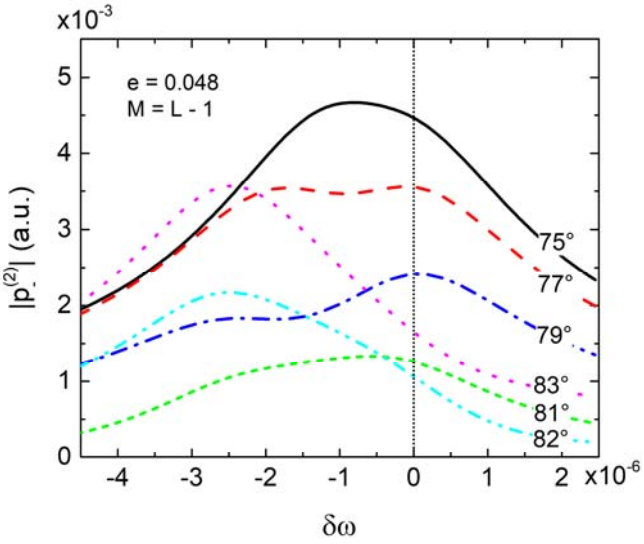

FIG. 8. Dependence of the $p_{-}^{(2)}$ coefficient on the offset from the resonator's frequency ($\delta\omega = 0$) for a set of the polar angles θ_p, $M = L-1$ and $e = 0.048$

B. Resonances of the scattered power

Experimental detection of frequencies of WGM resonances is usually based upon observation of the minima of the intensity of light transmitted through the fiber used to excite the resonances [1,82,83,85]. These minima correspond to frequencies at which the transfer of energy from the fiber to the resonator is at maximum. Under the steady-state conditions these frequencies also correspond to the maxima of the power scattered by the resonator (or by the resonator-particle system). These arguments, of course, do not take into account the coupling coefficient between the fiber and the resonator, which affects the excitation of the WGMs, as well as coupling of the scattered light back to the fiber. This coupling has been studied intensively for a single resonator [85–89], but how the presence of the particle affects the coupling, and conversely, how proximity of the taper affects the particle-induced effects, is not clear. There are some indications, however, that the effects due to interaction with particles can be stronger than the effects due to the taper [87], and while this question deserves more careful consideration one can assume that calculations of the scattered power in the absence of the fiber well represent the results of actual observations. This quantity provides more information about the resonator-particle interaction: in addition to the positions of the particle-induced resonances we can also see their widths and relative heights. Besides, this quantity allows us to predict whether the particle-induced resonances can be resolved.

The (dimensionless) power scattered by the resonator with a single WGM with a given polar number is given by the following expression

$$W_{sc}^{(\sigma)} = \sum_{l=1}^{l_{\max}} \left\{ \left| c_{0,l}^{(\sigma)} \right|^2 + \left| g_{0,l}^{(\sigma)} \right|^2 + \frac{1}{2} \sum_{m=1}^{l} \left(\left| c_{m+,l}^{(\sigma)} \right|^2 + \left| c_{m-,l}^{(\sigma)} \right|^2 + \left| g_{m+,l}^{(\sigma)} \right|^2 + \left| g_{m-,l}^{(\sigma)} \right|^2 \right) \right\}, \tag{29}$$

where the sum cut-off number $l_{\max}$ is chosen to achieve the convergence of the sum, and coefficients $c_{m\pm,l}^{(\sigma)}$ and $g_{m\pm,l}^{(\sigma)}$ are defined similarly to coefficients $p_{\pm 1}^{(\sigma)}$:

$$\begin{aligned} c_{m\pm,l}^{(\sigma)} &\equiv c_{m,l}^{(\sigma)} \pm c_{-m,l}^{(\sigma)} \\ g_{m\pm,l}^{(\sigma)} &\equiv g_{m,l}^{(\sigma)} \pm g_{-m,l}^{(\sigma)} \end{aligned} . \tag{30}$$

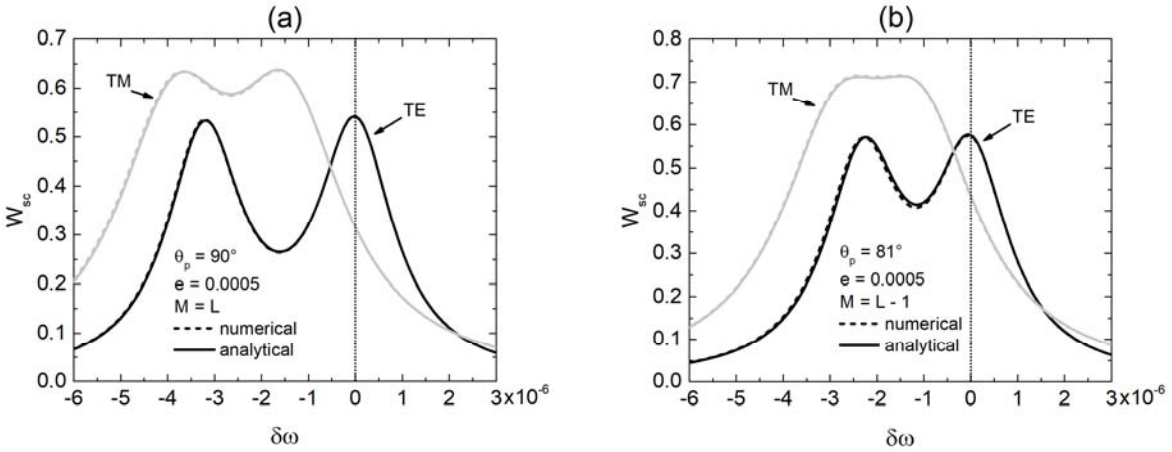

FIG. 9. Dependence of the scattered power on the frequency close to the resonator's frequency ($\delta\omega = 0$) for $e = 0.0005$ Graph (a) shows results for fundamental resonator's mode $M = L = 39$ and particle located at the equator, while graph (b) represents results for $M = L - 1 = 38$ and particle located at polar angle $\theta_p = 81°$. Solid lines correspond to analytical results and dashed lines correspond to numerical results obtained from Eq. (29).

Preliminary determination of the resonance positions based on computation of coefficients $p_{\pm 1}^{(\sigma)}$ makes finding resonances of the scattered power much more efficient as it significantly limits the range of frequencies that need to be covered. In Figure 9 we show how analytical results of the resonant approximation compare with numerical calculations for the resonator with small ellipticity $e = 0.0005$.

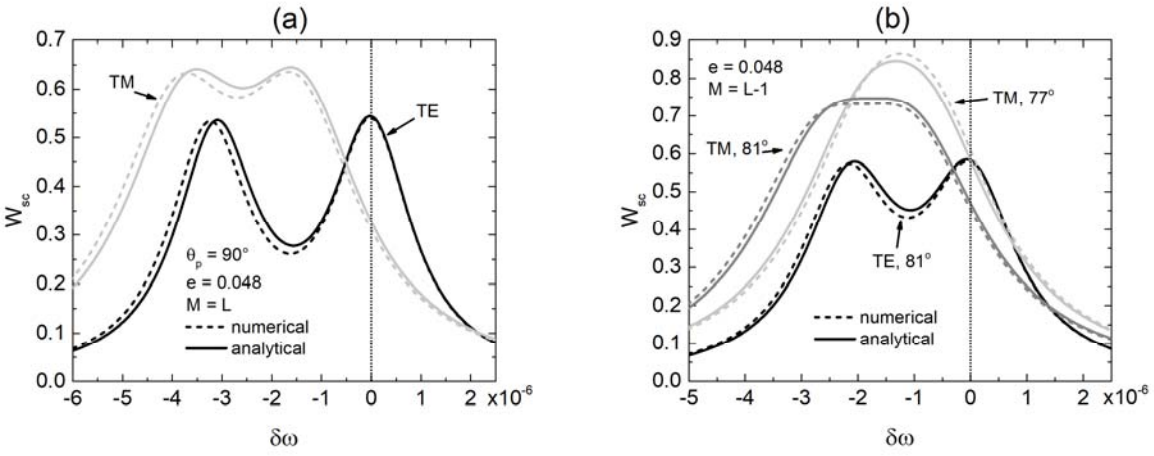

FIG. 10. Dependence of the resonator scattered power on the frequency close to the resonator's frequency ($\delta\omega = 0$) for $e = 0.048$. Graph (a) shows results for fundamental resonator's mode $M = L = 39$ and particle located at the equator, while graph (b) represents results for $M = L - 1 = 38$ and particle located at polar angles $\theta_p = 81°$ and $77°$. Solid lines correspond to analytical results and dashed lines correspond to numerical results obtained from Eq. (29) .

Analytical results are found to be in a good agreement with numerical simulations. For TE (TM)

mode in the selected frequency ranges the main contribution to the sum in Eq. (29) comes from $c^{(\sigma)}_{m\pm,l}$ ($g^{(\sigma)}_{m\pm,l}$) coefficients, while the rest coefficients are, at least, 4 orders of magnitude smaller, thus confirming the validity of the resonant approximation. Figure 10 shows the same quantities, but for ellipticity $e = 0.048$. One can see that with deviation of the particle from the equatorial

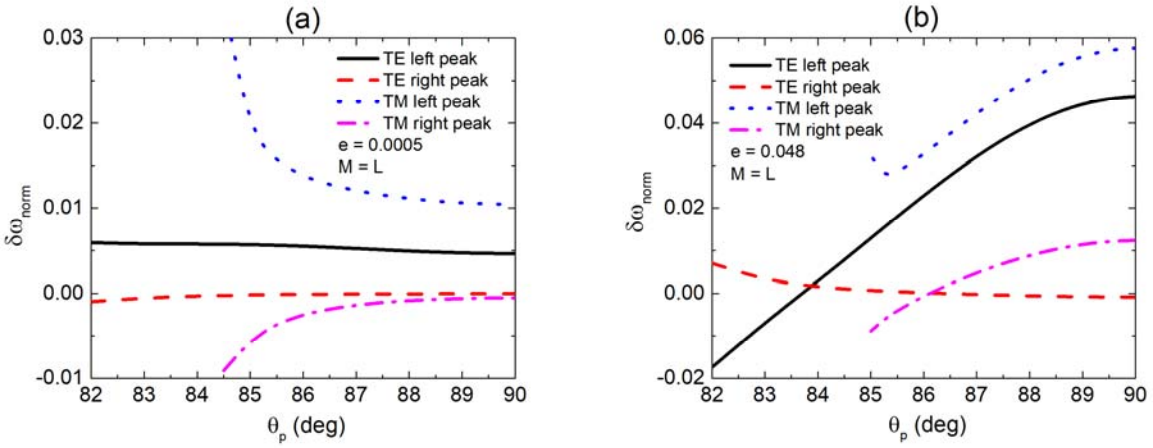

FIG. 11. Dependence of difference of peak positions of scattered power between the results of analytical approximation and numerical simulation on the angular position of the particle. Frequency difference is normalized on the modulus of the shift of the left peak from resonator's frequency at $\theta_p = 90°$ (see Figure 9(a) and Figure 10(a)) for fundamental mode $M = L = 39$. Graph (a) corresponds to $e = 0.0005$ and graph (b) is for $e = 0.048$. Curves for TM mode are calculated down to the angle of ~85° where both peaks merge together, while TE peaks are still separated even at 82°.

position the maxima of the scattered power move toward each other signifying decreasing separation between the resonance frequencies, and starting with some critical angle, different for TE and TM polarizations, the maxima start overlapping and merge into a single peak.

As expected, in the case of larger ellipticity the discrepancy between analytical and numerical results becomes more prominent. In order to achieve a better quantitative understanding of the significance of this difference we compared numerical and analytical results for the positions of the resonance maxima. The differences between these quantities as functions of the particle's position are shown in Figure 11, where they are normalized by the deviation of the frequency of the left peak from resonator's frequency at the equatorial position of the particle. One can see that the non-resonant terms in the T-matrix, which are taking into account in our numerical computations, result in corrections to the amount of the frequency splitting as large as $4 \div 6\%$ of the splitting, which is experimentally significant. One can also notice that the discrepancy between analytical and numerical results is greater when the deviations of the particle-induced resonances from the initial resonator's frequency are larger and decreases as the splitting of the resonances becomes smaller.

One of the interesting particle-induced effects found in spherical resonators [49] is a directionality of the scattered field determined by the position of the particle. Computing the dependence of the scattered intensity upon azimuthal angle in the equatorial plane of the spheroidal resonator, we found that even slight deviations from sphericity completely washes out

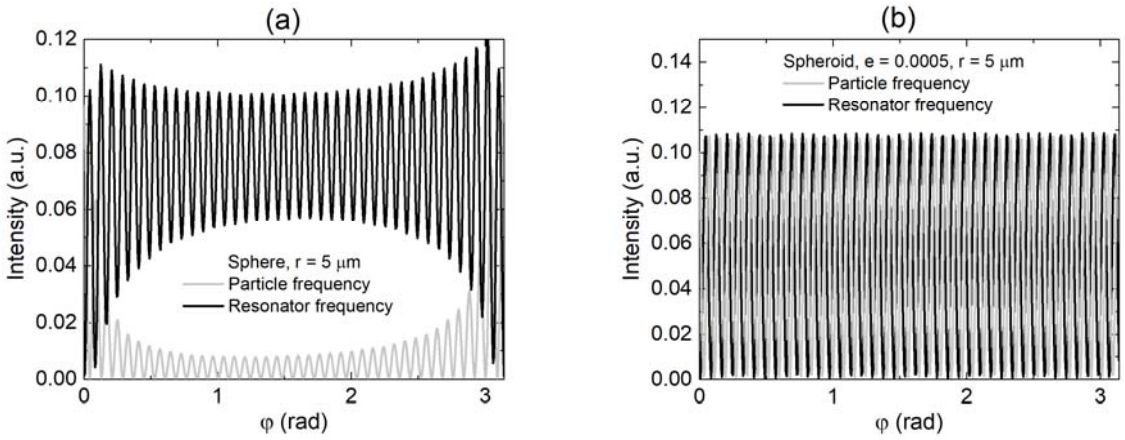

FIG. 12. Azimuthal intensity pattern in the equatorial plane for the sphere (a) and spheroid with $e = 0.0005$ (b) at radius $r = 5\mu m$ from the center. Angle is defined with respect to Z_p axis with particle located on equator.

this directionality (see Figure 12).

IV. CONCLUSIONS

In this paper we presented the computationally efficient numerical method of determining spectral characteristics of a spheroidal whispering-gallery-mode resonator interacting with a dielectric nanoparticle. The approach is based on combination of T-matrix formalism for a single resonator with a dipole approximation for a field of the nanoparticle and allows computing scattered field of the resonator-particle system illuminated by an incident field in the form of a single WGM mode of TE or TM polarization. This form of the incident field mimics excitation of the resonances by a tapered fiber. Our calculations showed that even smallest deviation of the resonator's shape from an ideal sphere renders spherical approximation for the shape of the resonator invalid and that the analytical resonant approximation for spheroidal resonances developed in Ref. [67,68] gives an accurate description of the spectral characteristics of the resonator-particle system. However, our calculations also showed that for the values of the ellipticity parameter of the order of 3-5%, which is typical for many nominally spherical resonators used in experiments, the corrections due to non-resonant elements of the T-matrix can become quite significant and result in up to 4-6% deviations of the resonant frequencies from the

values predicted by the resonant approximation. With particle-induced spectral modifications of the WGM resonances becoming a centerpiece of new sensing applications these corrections are important enough to take into account when using experimental results to size the nanoparticle analytes [14–16]. A direct comparison with presently available experimental data would require expanding the codes for calculation of the elements of T-matrix beyond available precision, which is possible, but lies beyond the scope of this work.

ACKNOWLEDGMENTS

Authors gratefully acknowledge financial support of the National Science Foundation via award # 1711801.

APPENDIX A: LORENTZ-MIE COEFFICIENTS FOR A SINGLE SPHERE

The Lorentz-Mie coefficients for ideal spheres are given by Eq. (5) of the main text, where respective functions $\beta_l^{(\sigma)}(x)$ and $\varsigma_l^{(\sigma)}$ are defined as

TE polarization:

$$\begin{aligned}\beta_l^{(1)}(x) &= y_l(n_1 x)\left[n_r x\, j_l(n_r x)\right]' - j_l(n_r x)\left[n_1 x\, y_l(n_1 x)\right]' \\ \varsigma_l^{(1)}(x) &= j_l(n_1 x)\left[n_r x\, j_l(n_r x)\right]' - j_l(n_r x)\left[n_1 x\, j_l(n_1 x)\right]'\end{aligned}, \tag{A1}$$

TM polarization:

$$\begin{aligned}\beta_l^{(2)}(x) &= \frac{n_1}{n_r} y_l(n_1 x)\left[n_r x\, j_l(n_r x)\right]' - \frac{n_r}{n_1} j_l(n_r x)\left[n_1 x\, y_l(n_1 x)\right]' \\ \varsigma_l^{(2)}(x) &= \frac{n_1}{n_r} j_l(n_1 x)\left[n_r x\, j_l(n_r x)\right]' - \frac{n_r}{n_1} j_l(n_r x)\left[n_1 x\, j_l(n_1 x)\right]'\end{aligned}. \tag{A2}$$

In Eqs. (A1) and (A2), functions $j_l(z), y_l(z)$ are spherical Bessel functions of the first and second kind respectively; $\left[zf(z)\right]'$ means differentiation with respect to the entire argument.

APPENDIX B: PROPERTIES OF T-MATRIX

Properties of T-matrix here are cited from Ref. [62].
The following relation is valid for a scatterer of an arbitrary shape and for any choice of the coordinate system. (Scatterer here is any object interacting with an incident electromagnetic wave. In the context of this paper, the role of the scatterer is assigned to the resonator.)

$$T_{m,l;\mu,\nu}^{(\sigma,\sigma')} = (-1)^{m+\mu}\, T_{-\mu,\nu;-m,l}^{(\sigma',\sigma)} \tag{B1}$$

For axially symmetrical scatterers additional relations between elements of T-matrix appear. In the resonator's coordinate system they can be expressed as

$$\begin{aligned}\tilde{T}^{(\sigma,\sigma')}_{m,l;m,\nu} &= (-1)^{\sigma+\sigma'}\,\tilde{T}^{(\sigma,\sigma')}_{-m,l;-m,\nu} \\ \tilde{T}^{(1,2)}_{0,l;0,\nu} &= \tilde{T}^{(2,1)}_{0,l;0,\nu} = 0\end{aligned}. \tag{B2}$$

Finally, the presence of the plane of symmetry perpendicular to the axis of rotation is responsible for the following relations between elements of the T-matrix in the resonator's coordinate system (for $\sigma \neq \sigma'$):

$$\begin{aligned}\tilde{T}^{(\sigma,\sigma)}_{m,l;m,\nu} &= \frac{1}{2}\left[1+(-1)^{l+\nu}\right]\,\tilde{T}^{(\sigma,\sigma)}_{m,l;m,\nu} \\ \tilde{T}^{(\sigma,\sigma')}_{m,l;m,\nu} &= \frac{1}{2}\left[1-(-1)^{l+\nu}\right]\,\tilde{T}^{(\sigma,\sigma')}_{m,l;m,\nu}\end{aligned}. \tag{B3}$$

Most important for us is the transformation property of the T-matrix expressed by Eq. (8) of the main text. Wigner D-matrix $D^{(\nu)}_{m,\mu}(\alpha,\beta,\gamma)$ appearing in that formula can be written down as

$$D^{(\nu)}_{m,\mu}(\alpha,\beta,\gamma) = e^{-im\alpha} d^{(\nu)}_{m,\mu}(\beta)\, e^{i\mu\gamma}, \tag{B4}$$

where $d^{(\nu)}_{m,\mu}(\beta)$ is called Wigner (small) d-matrix. One of its multiple representations is as follows

$$\begin{aligned}d^{(l)}_{m,m_1}(\beta) = \frac{1}{2^l}\sqrt{(l+m_l)!(l-m_l)!(l-m)!(l+m)!}\times \\ \sum_k (-1)^k \frac{\cos(\beta/2)^{2l-2k+m-m_1}\sin(\beta/2)^{2k-m+m_1}}{k!(l-m_l-k)!(k-m+m_l)!(l+m-k)!}\end{aligned}, \tag{B5}$$

where summation is carried over such k, which results in non-negative factorials in the denominator of Eq. (B5). Matrix $d^{(l)}_{m,m_l}(\beta)$ as a function of β has its maximum at $\beta = \pm\pi/2$, and decreases to zero when β approaches values of zero or $\pm\pi$. It has following important properties

$$d^{(l)}_{m,m_1}(-\beta) = (-1)^{m-m_1} d^{(l)}_{m,m_1}(\beta) \tag{B6}$$

and

$$d^{(l)}_{m,m_1}(\beta) = (-1)^{m-m_1} d^{(l)}_{m_1,m}(\beta) = d^{(l)}_{-m_1,-m}(\beta) \tag{B7}$$

valid for an arbitrary angle. In the particular case of $\beta = \pi/2$, Eq. (B5) gives

$$d^{(l)}_{m,m_1}(\pi/2)=\sqrt{(l+m_1)!(l-m_1)!(l-m)!(l+m)!}\times \sum_k \frac{(-1)^k}{k!(l-m_1-k)!(k-m+m_1)!(l+m-k)!}. \tag{B8}$$

In this case one can derive an additional relation

$$d^{(l)}_{-m,m_1}(\pi/2)=(-1)^{l-m_1}\,d^{(l)}_{m,m_1}(\pi/2), \tag{B9}$$

which allows for significant simplifications of the calculations of the T-matrix in the particle's coordinate system when the particle is at the equatorial position.

APPENDIX C: VECTOR SPHERICAL HARMONICS AND TRANSLATION COEFFICIENTS

Different normalizations for VSHs result in different definitions of the translation coefficients. To avoid possible confusion we present here relevant expressions used in this work, which are taken from Ref. [62]. It should be noted that the authors of Ref. [50] utilize different convention with regard to normalization of VSH, and, hence, use different formulas for the translation coefficients.

VSHs are functions of spherical coordinates r,θ,φ (radial, polar and azimuthal coordinates, respectively) defined with respect to a particular coordinate system. For TE polarization they are defined as

$$\begin{Bmatrix}\mathbf{M}^{(3)}_{m,l}(r,\theta,\varphi)\\ \mathbf{M}^{(1)}_{m,l}(r,\theta,\varphi)\end{Bmatrix}=\kappa_{m,l}\mathbf{C}_{m,l}(\theta,\varphi)\begin{Bmatrix}h^{(1)}_l(kr)\\ j^{(1)}_l(kr)\end{Bmatrix}, \tag{C1}$$

where

$$\kappa_{m,l}=\sqrt{\frac{(2l+1)(l-m)!}{4\pi l(l+1)(l+m)!}}. \tag{C2}$$

The angular portion of the VSH is defined as

$$\mathbf{C}_{m,l}(\theta,\varphi)=\left[i\mathbf{e}_\theta\frac{m}{\sin\theta}P^m_l(\cos\theta)-\mathbf{e}_\varphi\frac{d}{d\theta}P^m_l(\cos\theta)\right]e^{im\varphi}, \tag{C3}$$

where $\mathbf{e}_\theta,\mathbf{e}_\varphi$ are unit vectors of the spherical coordinate system for the polar and azimuthal directions, respectively, and $P^m_l(x)$ are standard associated Legendre functions. VSH of TM polarization are defined as

$$\begin{cases}\mathbf{N}_{m,l}^{(3)}(r,\theta,\varphi)\\ \mathbf{N}_{m,l}^{(1)}(r,\theta,\varphi)\end{cases}=\frac{1}{k}\nabla\times\begin{cases}\mathbf{M}_{m,l}^{(3)}(r,\theta,\varphi)\\ \mathbf{M}_{m,l}^{(1)}(r,\theta,\varphi)\end{cases}. \tag{C4}$$

Translation coefficients $A_{\mu,\nu;m,l}^{(+)}\left(k_1,\mathbf{d}_{pr}\right)$ and $B_{\mu,\nu;m,l}^{(+)}\left(k_1,\mathbf{d}_{pr}\right)$, which are consistent with definition of VSHs given by Eqs. (C1) - (C4), are expressed as functions of the radial d_{pr}, polar θ_{pr} and azimuthal φ_{pr} coordinates of the particle's position vector $\mathbf{d}_{pr}$ with respect to the center of the resonator.

$$\begin{aligned}A_{\mu,\nu;m,l}^{(+)}\left(k_1d_{pr},\theta_{pr},\varphi_{pr}\right)&=\frac{\kappa_{m,l}}{\kappa_{\mu,\nu}}(-1)^{\mu}\sum_{p=|l-\nu|}^{l+\nu}a(m,l\,|-\mu,\nu\,|\,p)a(l,\nu,p)h_p^{(1)}(kd_{pr})\times\\&\quad\times P_p^{m-\mu}\left(\cos\theta_{pr}\right)\exp\left[i\left(m-\mu\right)\varphi_{pr}\right]\\B_{\mu,\nu;m,l}^{(+)}\left(k_1d_{pr},\theta_{pr},\varphi_{pr}\right)&=\frac{\kappa_{m,l}}{\kappa_{\mu,\nu}}(-1)^{\mu+1}\sum_{p=|l-\nu|}^{l+\nu}a(m,l\,|-\mu,\nu\,|\,p,p-1)\,\mathrm{b}(l,\nu,p)h_p^{(1)}(kd_{pr})\times\\&\quad\times P_p^{m-\mu}\left(\cos\theta_{pr}\right)\exp\left[i\left(m-\mu\right)\varphi_{pr}\right]\end{aligned}, \tag{C5}$$

where

$$\begin{aligned}a(m,l\,|\,\mu,\nu\,|\,p)&=(-1)^{m+\mu}(2p+1)\sqrt{\frac{(l+m)!(\nu+\mu)!(p-m-\mu)!}{(l-m)!(\nu-\mu)!(p+m+\mu)!}}\\&\quad\times\begin{pmatrix}l&\nu&p\\m&\mu&-(m+\mu)\end{pmatrix}\begin{pmatrix}l&\nu&p\\0&0&0\end{pmatrix}\\a(m,l\,|\,\mu,\nu\,|\,p,q)&=(-1)^{m+\mu}(2p+1)\sqrt{\frac{(l+m)!(\nu+\mu)!(p-m-\mu)!}{(l-m)!(\nu-\mu)!(p+m+\mu)!}}\\&\quad\times\begin{pmatrix}l&\nu&p\\m&\mu&-(m+\mu)\end{pmatrix}\begin{pmatrix}l&\nu&q\\0&0&0\end{pmatrix}\end{aligned}, \tag{C6}$$

$$\begin{aligned}a(l,\nu,p)&=\frac{(i)^{\nu-l+p}(2\nu+1)}{2\nu(\nu+1)}\left[l(l+1)+\nu(\nu+1)-p(p+1)\right]\\\mathrm{b}(l,\nu,p)&=-\frac{(i)^{\nu-l+p}(2\nu+1)}{2\nu(\nu+1)}\sqrt{(l+\nu+p+1)(l+\nu-p+1)(l-\nu+p)(-l+\nu+p)}\end{aligned} \tag{C7}$$

and the coefficients

$$\begin{pmatrix}l&\nu&p\\m&\mu&-(m+\mu)\end{pmatrix} \tag{C8}$$

are Wigner 3j symbols. In the particle coordinate system $\theta_{pr}=0$ and, as a result, only $m=\mu$ components of the translation coefficients are different from zero. In the particular case, when one of the angular momentum indexes is taken to be unity, expressions for the translation coefficients simplify and become

$$A^{(+)}_{\mu,\nu;\mu,1}(k_1\mathbf{r}_{pr})=\sqrt{\frac{3}{2}}\left[\sqrt{\frac{(\nu+1)(\nu+|\mu|)}{(2\nu+1)(1+|\mu|)}}h^{(1)}_{\nu-1}(k_1r_{pr})+(-1)^{\mu}\sqrt{\frac{\nu(\nu+1-|\mu|)}{(2\nu+1)(1+|\mu|)}}h^{(1)}_{\nu+1}(k_1r_{pr})\right] \quad \text{(C9)}$$

$$B^{(+)}_{\mu,\nu;\mu,1}(k_1\mathbf{r}_{pr})=\mathrm{i}\frac{\sqrt{3}}{2}\mu\sqrt{2\nu+1}h^{(1)}_{\nu}(k_1r_{pr})$$

[1] A. B. Matsko and V. S. Ilchenko, IEEE J. Sel. Top. Quantum Electron. **12**, 3 (2006).

[2] A. N. Oraevsky, Quantum Electron. **32**, 377 (2002).

[3] F. Vollmer, S. Arnold, and D. Keng, Proc. Natl. Acad. Sci. U. S. A. **105**, 20701 (2008).

[4] S. I. Shopova, R. Rajmangal, Y. Nishida, and S. Arnold, Rev. Sci. Instrum. **81**, 103110 (2010).

[5] W. Kim, S. K. Ozdemir, J. Zhu, and L. Yang, Appl. Phys. Lett. **98**, 141106 (2011).

[6] J. Knittel, T. G. McRae, K. H. Lee, and W. P. Bowen, Appl. Phys. Lett. **97**, 123704 (2010).

[7] J. D. Swaim, J. Knittel, and W. P. Bowen, Appl. Phys. Lett. **99**, 243109 (2011).

[8] M. A. Santiago-Cordoba, S. V Boriskina, F. Vollmer, and M. C. Demirel, Appl. Phys. Lett. **99**, 73701 (2011).

[9] L. Shao, X.-F. Jiang, X.-C. Yu, B.-B. Li, W. R. Clements, F. Vollmer, W. Wang, Y.-F. Xiao, and Q. Gong, Adv. Mater. **25**, 5616 (2013).

[10] Ş. K. Özdemir, J. Zhu, X. Yang, B. Peng, H. Yilmaz, L. He, F. Monifi, S. H. Huang, G. L. Long, and L. Yang, Proc. Natl. Acad. Sci. U. S. A. **111**, E3836 (2014).

[11] B.-B. Li, W. R. Clements, X.-C. Yu, K. Shi, Q. Gong, and Y.-F. Xiao, Proc. Natl. Acad. Sci. **111**, 14657 (2014).

[12] D. Keng, X. Tan, and S. Arnold, Appl. Phys. Lett. **105**, 071105 (2014).

[13] S. I. Shopova, R. Rajmangal, S. Holler, and S. Arnold, Appl. Phys. Lett. **98**, 243104 (2011).

[14] V. R. Dantham, S. Holler, V. Kolchenko, Z. Wan, and S. Arnold, Appl. Phys. Lett. **101**, 043704 (2012).

[15] V. R. Dantham, S. Holler, C. Barbre, D. Keng, V. Kolchenko, and S. Arnold, Nano Lett. **13**, 3347 (2013).

[16] J. G. Zhu, S. K. Ozdemir, Y. F. Xiao, L. Li, L. N. He, D. R. Chen, and L. Yang, Nat. Photonics **4**, 46 (2010).

[17] W. Kim, S. K. Ozdemir, J. Zhu, L. He, and L. Yang, Appl. Phys. Lett. **97**, 71111 (2010).

[18] L. He, Ş. K. Özdemir, J. Zhu, and L. Yang, Phys. Rev. A **82**, 053810 (2010).

[19] L. N. He, S. K. Ozdemir, J. G. Zhu, W. Kim, L. Yang, K. Ozdemir, J. G. Zhu, W. Kim, and L. Yang, Nat. Nanotechnol. **6**, 428 (2011).

[20] J. G. Zhu, S. K. Ozdemir, L. He, D. R. Chen, and L. Yang, Opt. Express **19**, 16195 (2011).

[21] D. Alton, N. Stern, T. Aoki, H. Lee, E. Ostby, K. J. Vahala, and H. J. Kimble, Nat. Phys. **7**, 159 (2011).

[22] C. P. Dettmann, G. V Morozov, M. Sieber, and H. Waalkens, Phys. Rev. A (Atomic, Mol. Opt. Physics) **80**, 63813 (2009).

[23] N. Zhang, S. Liu, K. Wang, Z. Gu, M. Li, N. Yi, S. Xiao, and Q. Song, Sci. Rep. **5**, 11912 (2015).

[24] Q. Song and H. Cao, Opt. Lett. **36**, 103 (2011).

[25] P. G. Schiro and A. S. Kwok, Opt. Express **12**, (2004).

[26] S. V Boriskina and B. M. Reinhard, Proc. Natl. Acad. Sci. U. S. A. **108**, 3147 (2011).

[27] S. Arnold, D. Keng, S. I. Shopova, S. Holler, W. Zurawsky, and F. Vollmer, Opt. Express **17**, 6230 (2009).

[28] H. Cai and A. W. Poon, Opt. Lett. **35**, 2855 (2010).

[29] H. Cai and A. W. Poon, Opt. Lett. **36**, 4257 (2011).

[30] A. García-Etxarri, R. Gómez-Medina, L. S. Froufe-Pérez, C. López, L. Chantada, F. Scheffold, J. Aizpurua, M. Nieto-Vesperinas, and J. J. Sáenz, Opt. Express **19**, 4815 (2011).

[31] P. Kapitanova, V. Ternovski, A. Miroshnichenko, N. Pavlov, P. Belov, Y. Kivshar, and M. Tribelsky, Sci. Rep. **7**, 731 (2017).

[32] M. I. Tribelsky and A. E. Miroshnichenko, Phys. Rev. A **93**, 053837 (2016).

[33] D. A. Smirnova, A. B. Khanikaev, L. A. Smirnov, and Y. S. Kivshar, 19 (2016).

[34] Z. Y. Jia, J. N. Li, H. W. Wu, C. Wang, T. Y. Chen, R. W. Peng, and M. Wang, J. Appl. Phys. **119**, 074302 (2016).

[35] C. Wang, Z. Y. Jia, K. Zhang, Y. Zhou, R. H. Fan, X. Xiong, and R. W. Peng, J. Appl. Phys. **115**, 244312 (2014).

[36] D. S. Weiss, V. Sandoghdar, J. Hare, V. Lefèvre-Seguin, J.-M. Raimond, and S. Haroche, Opt. Lett. **20**, 1835 (1995).

[37] M. L. Gorodetsky, A. D. Pryamikov, and V. S. Ilchenko, J. Opt. Soc. Am. B **17**, 1051 (2000).

[38] A. Mazzei, S. Goetzinger, L. D. Menezes, G. Zumofen, O. Benson, and V. Sandoghdar, Phys. Rev. Lett. **99**, 173603 (2007).

[39] S. Arnold, M. Khoshsima, I. Teraoka, S. Holler, and F. Vollmer, Opt. Lett. **28**, 272 (2003).

[40] F. Vollmer, D. Braun, A. Libchaber, M. Khoshsima, I. Teraoka, and S. Arnold, Appl.

Phys. Lett. **80**, 4057 (2002).

[41] S. Arnold, S. I. Shopova, and S. Holler, Opt. Express **18**, 281 (2010).

[42] J. Zhu, ahin K. Özdemir, L. He, and L. Yang, Opt. Express **18**, 23535 (2010).

[43] X. Yi, Y.-F. Xiao, Y.-C. Liu, B.-B. Li, Y.-L. Chen, Y. Li, and Q. Gong, Phys. Rev. A **83**, 23803 (2011).

[44] Y.-C. Liu, Y.-F. Xiao, B.-B. Li, X.-F. Jiang, Y. Li, and Q. Gong, Phys. Rev. A **84**, 11805 (2011).

[45] Y. Shen, Phys. Rev. A **85**, (2012).

[46] T. Tudorovskiy, R. Höhmann, U. Kuhl, and H.-J. Stöckmann, J. Phys. A Math. Theor. **41**, 275101 (2008).

[47] L. Deych, M. Ostrowski, and Y. Yi, Opt. Lett. **36**, 3154 (2011).

[48] L. Deych and J. Rubin, Phys. Rev. A **80**, 061805 (2009).

[49] J. T. Rubin and L. Deych, Phys. Rev. A **81**, 53827 (2010).

[50] M. R. Foreman and F. Vollmer, New J. Phys. **15**, 083006 (2013).

[51] O. C. Zienkiewicz, R. L. Taylor, and J. Z. Zhu:, *The Finite Element Method: Its Basis and Fundamentals, Sev 9781856176330: Amazon.Com: Books*, Seventh Ed (Butterworth-Heinemann, 2013).

[52] A. Taflove and S. C. Hagness, *Computational Electrodynamics: The Finite-Difference Time-Domain Method*, Third Edit (Artech House, 2005).

[53] M. Oxborrow, in *IEEE Trans. Microw. Theory Tech.* (2007), pp. 1209–1218.

[54] A. Kaplan, M. Tomes, T. Carmon, M. Kozlov, O. Cohen, G. Bartal, and H. G. L. Schwefel, Opt. Express **21**, 14169 (2013).

[55] J. Krupka, D. Cros, A. Luiten, and M. Tobar, Electron. Lett. Online **32**, 0 (1996).

[56] J. Krupka, D. Cros, M. Aubourg, and P. Guillon, IEEE Trans. Microw. Theory Tech. **42**, 56 (1994).

[57] I. Breunig, B. Sturman, F. Sedlmeir, H. G. L. Schwefel, and K. Buse, Opt. Express **21**, 30683 (2013).

[58] P. Barber and C. Yeh, Appl. Opt. **14**, 2864 (1975).

[59] M. L. Burrows, Electron. Lett. **5**, 277 (1969).

[60] L. Bi, P. Yang, G. W. Kattawar, and M. I. Mishchenko, J. Quant. Spectrosc. Radiat. Transf. **123**, 17 (2013).

[61] P. W. Barber and S. C. Hill, *Light Scattering by Particles: Computational Methods* (World Scientific Publishing Company, Singapore, 1990).

[62] M. I. Mishchenko, L. D. Travis, and A. A. Lacis, *Scattering, Absorption, and Emission of Light by Small Particles* (Cambridge University Press, Cambridge□; New York, 2002).

[63] H. Lai, P. Leung, K. Young, P. Barber, and S. Hill, Phys. Rev. A **41**, 5187 (1990).

[64] M. I. Mishchenko, L. D. Travis, and A. A. Lacis, *Multiple Scattering of Light by Particles□: Radiative Transfer and Coherent Backscattering* (Cambridge University

Press, Cambridge□; New York, 2006).

[65] I. Teraoka, S. Arnold, and F. Vollmer, J. Opt. Soc. Am. B-Optical Phys. **20**, 1937 (2003).

[66] I. Teraoka and S. Arnold, J. Opt. Soc. Am. B **23**, 1381 (2006).

[67] L. Deych and V. Shuvayev, Phys. Rev. A **92**, 013842 (2015).

[68] L. Deych and V. Shuvayev, Opt. Lett. **40**, 4536 (2015).

[69] X. Li, C. Yang, D. Jia, Z. Cao, Q. Mu, L. Hu, Z. Peng, Y. Liu, L. Yao, and L. Xuan, Opt. Laser Technol. **54**, 284 (2013).

[70] N. Yi, S. S. Sun, Y. Gao, K. Wang, Z. Gu, S. S. Sun, Q. Song, and S. Xiao, Sci. Rep. **6**, 25760 (2016).

[71] A. I. Kuznetsov, A. E. Miroshnichenko, Y. H. Fu, J. Zhang, and B. Luk'yanchuk, Sci. Rep. **2**, 492 (2012).

[72] Lord Rayleigh (J.W. Strutt), Phil. Mag. **44**, 28 (1897).

[73] Lord Rayleigh (j.W. Strutt), Proc. R. Soc. London Ser. A **79**, 399 (1907).

[74] R. F. Millar, Radio Sci. **8**, 785 (1973).

[75] B. Suhai and G. Horváth, J. Opt. Soc. Am. A. Opt. Image Sci. Vis. **21**, 1669 (2004).

[76] P. Paul, Opt. Commun. **278**, 204 (2007).

[77] V. Jamnejad-Dailami, R. Mittra, and T. Itoh, IEEE Trans. Antennas Propag. **20**, (1972).

[78] P. van den Berg and J. Fokkema, IEEE Trans. Antennas Propag. **27**, (1979).

[79] A. V Tishchenko, Opt. Express **17**, 17102 (2009).

[80] O. R. Cruzan, Q. Appl. Math. **20**, 33 (1962).

[81] K. T. Kim, Prog. Electromagn. Res. **48**, 45 (2004).

[82] M. Cai, O. Painter, and K. J. Vahala, Phys. Rev. Lett. **85**, 74 (2000).

[83] M. L. Gorodetsky and V. S. Ilchenko, J. Opt. Soc. Am. B **16**, 147 (1999).

[84] T. J. Kippenberg, H. Rokhsari, T. Carmon, A. Scherer, and K. J. Vahala, Phys. Rev. Lett. **95**, (2005).

[85] S. Spillane, T. Kippenberg, O. Painter, and K. Vahala, Phys. Rev. Lett. **91**, 2 (2003).

[86] J. C. Knight, G. Cheung, F. Jacques, and T. A. Birks, Opt. Lett. **22**, 1129 (1997).

[87] C. L. Zou, Y. Yang, C. H. Dong, Y. F. Xiao, X. W. Wu, Z. F. Han, and G. C. Guo, J. Opt. Soc. Am. B-Optical Phys. **25**, 1895 (2008).

[88] B. E. Little, J. P. Laine, and H. A. Haus, J. Light. Technol. **17**, 704 (1999).

[89] M. J. Humphrey, E. Dale, A. T. Rosenberger, and D. K. Bandy, Opt. Commun. **271**, 124 (2007).

[90] M. Mishchenko, Http://Www.Giss.Nasa.Gov/Staff/Mmishchenko/T_matrix.Html (2013).

[91] S. Kaminski, L. L. Martin, and T. Carmon, Opt. Express **23**, 28914 (2015).

[92] S. Maayani, L. L. Martin, and T. Carmon, Nat. Commun. **7**, 10435 (2016).

[93] G. Bahl, K. H. Kim, W. Lee, J. Liu, X. Fan, and T. Carmon, Nat. Commun. **4**, 1994

(2013).

[94] S. Kaminski, L. L. Martin, S. Maayani, and T. Carmon, ArXiv Prepr. ArXiv1603.02218 (2016).

[95] S. T. Attar, V. Shuvayev, L. Deych, L. L. Martin, and T. Carmon, Opt. Express **24**, 13134 (2016).